AGU PUBLICATIONS

JGR

Journal of Geophysical Research: Solid Earth

RESEARCH ARTICLE
10.1002/2016JB013507

Key Points:
- Statistical modeling of the spatiotemporal earthquake occurrence: ETAS, Poisson, and Brownian Passage Time
- Quantification of the seismotectonic potential for Naples
- Bayesian hazard maps including the soil amplification effects

Supporting Information:
- Supporting Information S1

Correspondence to:
L. Faenza,
licia.faenza@ingv.it

Citation:
Faenza, L., S. Pierdominici, S. Hainzl, F. R. Cinti, L. Sandri, J. Selva, R. Tonini, and P. Perfetti (2017), A Bayesian seismic hazard analysis for the city of Naples, *J. Geophys. Res. Solid Earth*, *122*, 1990–2012, doi:10.1002/2016JB013507.

Received 2 SEP 2016
Accepted 24 DEC 2016
Accepted article online 29 DEC 2016
Published online 3 MAR 2017

A Bayesian seismic hazard analysis for the city of Naples

Licia Faenza[1], Simona Pierdominici[2], Sebastian Hainzl[2], Francesca Romana Cinti[3], Laura Sandri[4], Jacopo Selva[4], Roberto Tonini[3], and Paolo Perfetti[4]

[1]Istituto Nazionale Geofisica e Vulcanologia, Centro Nazionale Terremoti, Rome, Italy, [2]Helmholtz-Zentrum Potsdam Deutsches GeoForschungsZentrum GFZ, Potsdam, Germany, [3]Istituto Nazionale Geofisica e Vulcanologia, Rome, Italy, [4]Istituto Nazionale Geofisica e Vulcanologia, Bologna, Italy

Abstract In this paper we explore the feasibility of formulating the hazard assessment procedure to include the information of past earthquakes into the probabilistic seismic hazard analysis, together with the use of an ensemble modeling technique. This strategy allows, on the one hand, to enlarge the information used in the evaluation of the hazard, from alternative models for the earthquake generation process to past shaking and, on the other hand, to explicitly account for the uncertainties. The Bayesian scheme we propose is applied to evaluate the seismic hazard of Naples. The framework in which we have embedded the tools is flexible to include all types of uncertainties. Here we focus on a sensitive study of the earthquake occurrence by implementing models that span from random to cluster-type temporal behavior and models that include quasiperiodic occurrence of earthquakes on faults. We implement five different spatiotemporal models to parameterize the occurrence of earthquakes potentially dangerous for Naples. Subsequently, we combine these hazard curves with ShakeMaps of past earthquakes that have been felt in Naples since 1200 A.D. The results are posterior ensemble hazard curves for three exposure times, e.g., 5, 10, and 50 years, in a dense grid that covers the municipality of Naples, considering rocky soil and including the site amplification. Our results show the importance to include the data from past shaking since the difference between the prior and the posterior is about 8–15% for the different exposure times.

1. Introduction

The quantification of the seismic hazard is based on models to describe earthquake distributions in terms of time, space, and magnitude. Probabilistic seismic hazard assessment (PSHA hereinafter) is expressed as the quantification of the probability of exceeding a given ground motion intensity value in the exposure time window in a given area [*Senior Seismic Hazard Analysis Committee (SSHAC)*, 1997]. This approach is usually made on the basis of statistical modeling of earthquake occurrence and ground motion, where the latter is modeled through the so-called ground motion prediction equations, GMPEs, that predict the propagation of seismic waves through the Earth. In general, the PSHA explores all the available sources of earthquakes able to generate damage in the area of interest. However, the adoption of this strategy neglects the information on past shaking suffered in the area of interest which is instead included in the macroseismic intensity field on past earthquakes. In Italy, there is a long tradition on historical seismicity and the Italian Macroseismic Data Base (DBMI) [*Locati et al.*, 2011] is one of the most complete and homogeneous archives in terms of intensity reporting the shaking of earthquakes in the Italian Peninsula since 1000 B.C.

We believe that the inclusion of data from past shaking in PSHA could improve the quantification of the hazard. In this work we focus on an approach which combines the PSHA with the past data in the site of interest. The great advantage of this approach is the capability to better quantify the uncertainties and to make use of all the available information on the shaking in Naples. The combination of seismic hazard values and past shaking data is performed through the adoption of the Bayesian approach. "Bayesian inference is the process of fitting a probability model to a set of observations and summarizing the results with a probability distribution for the parameters of the model" [*Gelman et al.*, 2000]. Its applications span over several scientific and economical disciplines [*Marzocchi et al.*, 2004, 2008; *Faenza et al.*, 2010; *Grezio et al.*, 2010; *Selva and Sandri*, 2013], showing some interesting aspects. The two most relevant points are the possibility to simultaneously include heterogeneous sources of information on the process under prior beliefs and observations and to estimate the uncertainty of the results obtained. In the quantification of the seismic hazard the treatment of aleatory and epistemic uncertainties is of primary importance. In particular, the aleatory uncertainty is associated to

the intrinsic stochasticity of the process. This results in an unavoidable impossibility of deterministically predicting its evolution. The epistemic uncertainty represents our limited knowledge of the system. An overview of this aspect can be found in *Woo* [1999], *Field et al.* [2003], and *MacKay* [2003]. While in principle it is possible to reduce the epistemic type of uncertainty by increasing the number of data points or improving the physical knowledge of the phenomenon, the aleatoric one is independent on our degree of knowledge and cannot be lowered. Because of these features, Bayesian inference can be a useful instrument to quantify the probabilistic seismic hazard as recently proposed by *Selva and Sandri* [2013]. In their work, the authors explain the theoretical basis of the Bayesian framework in PSHA applications and its advantages.

This work implements the generic inference scheme for assessing the seismic hazard in Naples, one of the cities with the highest natural hazard in Italy. We focus on seismic hazard analysis in the exposure time of 5, 10, and 50 years, for the medium- and long-term mitigation analysis. We mainly focus on the inclusion of the uncertainties arising from the choice of different patterns of earthquake occurrence, ignoring the part about the GMPEs. We are aware that the GMPEs are one, if not the main, source of uncertainty in the seismic hazard assessment. In recent years, there has been a series of pioneering works of Scherbaum and coauthors [*Scherbaum et al.*, 2004, 2005, 2009; *Scherbaum and Kuehn*, 2011] on the proper selection of GMPEs to be used and the weight to be given to each model based on its performance. This opened the road to different methodologies for the scoring of the GMPEs (see the most recent works of *Kale and Akkar* [2013] and *Roselli et al.* [2016], for example). Although we ignore this in our present work, we want to emphasize that the Bayesian structure proposed here remains valid and flexible to the inclusion of new variables in the calculation of the hazard, such as the introduction of new GMPEs and their relative weights.

The paper starts from the description of the geological active faults in the area of interest and subsequently presents the general description of the methodology. In the latter part of the paper, the application to Naples and its results are described and discussed, as follows. First, we deal with the probabilistic quantification of the hazard through Monte Carlo simulation of seismic catalogs. Three factors contribute to the probabilistic description of earthquake occurrences — i.e., their distributions in time, space, and size — and we focus on the spatiotemporal occurrence here. Second, we constrain the uncertainties of the calculated hazard estimates by past shaking data. Finally, we aggregate the information coming from the different alternative hazard models by producing ensemble models.

2. Active Faults

In the last few years many studies have been focused on determination and definition of the seismic, volcanic, and tsunamogenic hazard in the city of Naples [*Faenza et al.*, 2013; *Selva et al.*, 2014; *Grezio et al.*, 2014]. The city of Naples with its neighboring area is one of the most densely populated places in Italy. In addition, the risk is increased by type and condition of buildings and monuments in the city. In light of this, it is crucial to assess which active faults could produce an earthquake able to be felt and damage Naples and the surrounding area (dashed box "a" in Figure 1). Two steps are followed: (i) gather the earthquake data set from macroseismic intensity database in order to list the events that have impact on the target area since historical time; (ii) build the fault data set using seismogenic source databases and publications in order to identify the active tectonic structures responsible for each of the "impacting" events (the set includes also faults with no documented activity but potentially hazardous for the city). Our analysis leads to a geological data set for the target area, and therefore not appropriate for hazard assessment of other regions.

2.1. Earthquake Data Sets

The Italian Macroseismic Intensity Database DBMI11 ([*Locati et al.*, 2011], 1000 A.D. – 2006 A.D.) is our source for the selection of earthquake data. Earthquake intensities in the database follow the Mercalli-Cancani-Sieberg, MCS, scale [*Sieberg*, 1930] in classes spaced by one unit (i.e., Is 4, 5, and 6). The criteria used for the selection are as follows: (i) counting the events striking Naples with intensity (Is) larger than or equal to 4; (ii) discarding the events when Is $<$ 4, Is = NF (not felt), and Is = RS (instrumental records, not suitable for microseismic study); (iii) encoding the events when simply reported as F (felt) and D (damaged), with intensity numerical values of Is = 4 and Is = 6, respectively; (iv) discarding the events likely related to phases of volcanic crisis (occurrence A.D. ages: i.e., 62, 79, 1760, 1883, 1916, and 1999). A minimum intensity Is = 4 represents the level of shaking that can be felt, while a value of Is = 6 represents the level of shaking that could damage the buildings. Following these criteria, a total of 48 earthquakes are selected with magnitudes from 4.7 to 7.0 and Is values in Naples between 4 and 8 (Table 1 and Figure 1). According to the historical database, Naples felt events occurring also at large distances, the farthest at about 400 km (dashed box "b" in Figure 1). We include

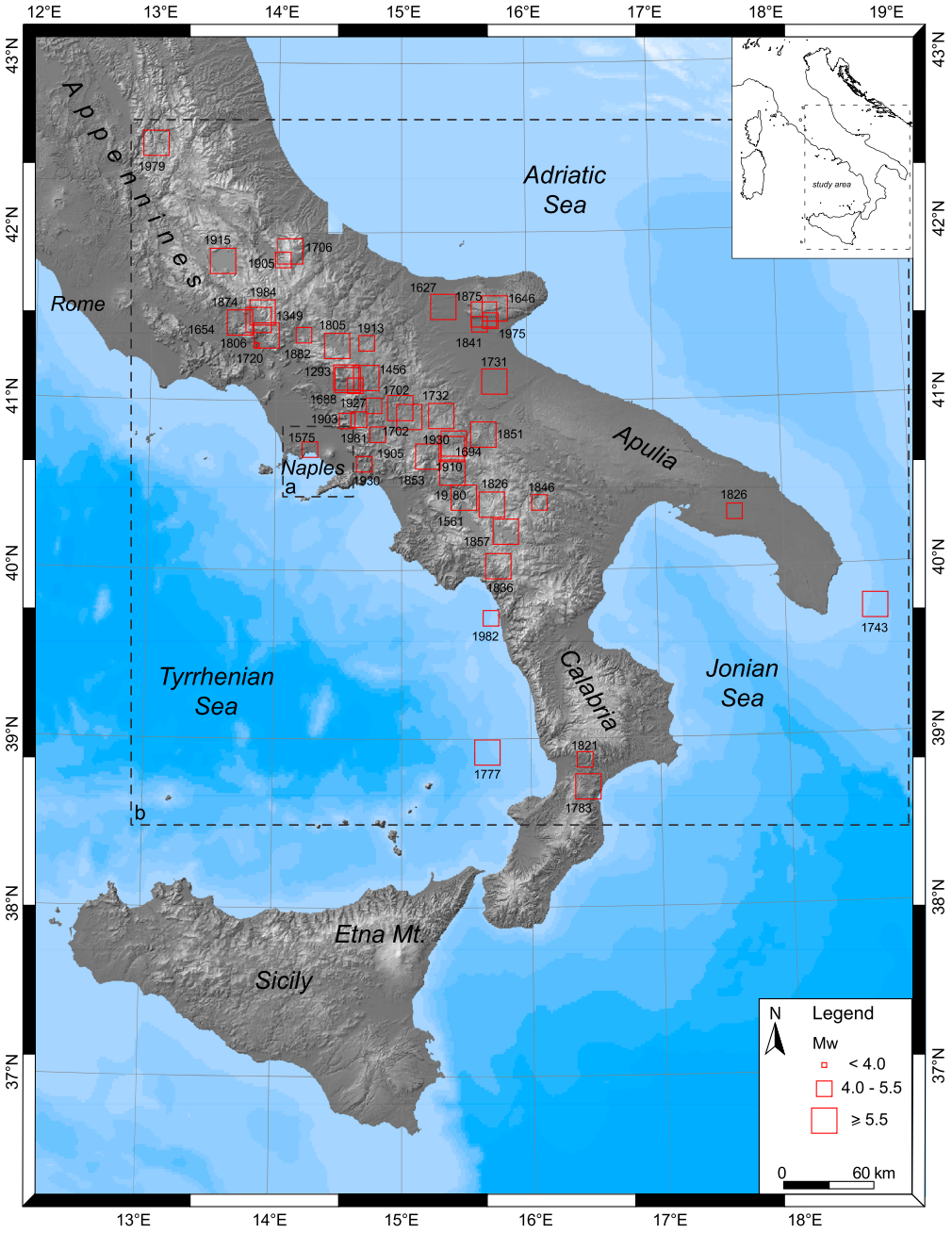

Figure 1. Spatial distribution of the seismic events felt in the city of Naples (DBMI11 catalog) [*Locati et al.*, 2011] (see also Table 1). The year of the earthquake occurrence is noted close to each red square. The dashed boxes "a" and "b" include felt earthquakes occurring at short and large distances.

these events and the relative causative faults in the modeling to be conservative; however, for their size and distance it may be inferred that some of these events are unlikely hazardous for Naples (e.g., 1743 Basso Ionio; 1821 Catanzaro; 1826 Manduria, and 1979 Valnerina earthquakes).

2.2. Fault Data

In this section we describe the fault selection and the reasoning used in the compilation. The aim of this selection is to make the data suitable for the simulation of seismic catalogs. We associated a fault to each of

Table 1. Seismic Events Felt in the City of Naples[a]

YY	MM	DD	HH	Mi	Se	Area	I_s	I_{mx}	Lat	Lon	I_o	M_w
1293	9	4				Sannio	7	9	41.304	14.548	8–9	5.78
1349	9	9	8	15		Lazio meridionale-Molise	7	10	41.560	13.901	10	6.59
1456	12	5				Molise	8	11	41.302	14.711	11	7.22
1561	8	19	15	50		Vallo di Diano	4–5	10–11	40.563	15.505	10	6.83
1575	6	5				Napoli	6–7	6–7	40.855	14.260	6–7	4.93
1627	7	30	10	50		Gargano	5	10	41.737	15.342	10	6.66
1646	5	31				Gargano	5	10	41.727	15.764	9–10	6.61
1654	7	24	0	25		Sorano-Marsica	F	10	41.635	13.683	9–10	6.29
1688	6	5	15	30		Sannio	8	11	41.283	14.561	11	6.98
1694	9	8	11	40		Irpinia-Basilicata	7	10	40.862	15.406	10	6.79
1702	3	14	4	30		Benevento	5	7–8	41.129	14.777	6–7	4.93
1702	3	14	5			Beneventano-Irpinia	6	10	41.120	14.989	10	6.54
1706	11	3	13			Maiella	4–5	10–11	42.076	14.080	10–11	6.83
1720	8	28				Cassino	5		41.490	13.814		4.80
1731	3	20	3			Foggiano	5	9	41.274	15.757	9	6.53
1732	11	29	7	40		Irpinia	7	10–11	41.064	15.059	10–11	6.64
1743	2	20	16	30		Basso Ionio	4–5	9	39.852	18.777	9	7.13
1777	6	6	16	15		Calabria	4–5		38.121	13.353	6	6.40
1783	3	28	18	55		Calabria	4	11	38.785	16.464	11	6.98
1805	7	26	21			Molise	7–8	10	41.500	14.474	10	6.62
1806	7	21	9			Cassino	F		41.490	13.814		5.10
1821	8	2				Catanzaro	F	7–8	38.944	16.452	7	5.14
1826	2	1	16			Basilicata	F	9	40.520	15.727	8	5.76
1826	10	26	18			Manduria	F	6–7	40.451	17.678	6–7	5.36
1836	11	20	7	30		Basilicata meridionale	5	9	40.142	15.776	8	6.02
1841	2	21				S. Marco in Lamis	F	7–8	41.626	15.639	6–7	5.27
1846	8	8				Campomaggiore	F	6–7	40.530	16.113	6–7	5.24
1851	8	14	13	20		Basilicata	5	10	40.952	15.667	10	6.38
1853	4	9	12	45		Irpinia	4	9	40.818	15.215	8	5.56
1857	12	16	21	15		Basilicata	6	11	40.352	15.842	11	7.03
1874	12	6	15	50		Monti della Meta	4	8	41.655	13.827	7–8	5.52
1875	12	6				S. Marco in Lamis	6–7	8	41.689	15.677	8	5.98
1882	6	6	5	40		Monti del Matese	5	8	41.558	14.204	7	5.27
1903	5	4	3	44		Valle Caudina	F	7–8	41.034	14.557	7	4.73
1905	8	25	20	41		Sulmona	F	7	42.019	14.026	6	5.16
1905	3	14	19	16		Beneventano	4–5	6–7	40.951	14.806	6–7	4.90
1910	6	7	2	4		Irpinia-Basilicata	4	9	40.898	15.421	8	5.73
1913	10	4	18	26		Matese	4	8	41.513	14.716	7–8	5.37
1915	1	13	6	52		Avezzano	5	11	42.014	13.530	11	7.00
1927	5	25	2	50	30	Cerreto	4	6–7	41.250	14.624	6	4.95
1930	7	23	0	8	43	Irpinia	7	10	41.068	15.318	10	6.62
1930	4	27	1	46		Salernitano	4	7	40.769	14.700		4.76
1975	6	19	10	11	14	Mattinatella	4	6	41.646	15.726	6	5.18
1979	9	19	21	35	37	Valnerina	4	8–9	42.730	12.956	8–9	5.86
1980	11	23	18	34	52	Irpinia-Basilicata	7	10	40.724	15.414	10	6.89
1981	2	14	17	27	46	Baiano	5–6	7–8	41.044	14.651	7–8	4.90
1982	3	21	9	44	2	Golfo di Policastro	4	7–8	39.834	15.747		5.36
1984	5	7	17	49	43	Appennino abruzzese	5–6	8	41.700	13.862	8	5.89

[a] I_s: site intensity; I_{mx}: maximum intensity at site; I_o: epicentral intensity; M_w: moment magnitude.

the seismic event of Table 1; the parameters of the fault geometry and kinematic (i.e., length, width, strike, dip, rake, minimum and maximum depth, and recurrence) were assigned accordingly to the event size and to the local tectonic setting. We consulted several literature sources to finalize this step, including the Database of Individual Seismogenic Source [*Database of Individual Seismogenic Source (DISS) Working Group*, 2015], the compilations of *Cinque et al.* [2000] and *Galadini et al.* [2001], and some specific published papers reporting more accurate or original geological data. When no documentation of fault/event is available in literature, we assigned the fault from scratch, according to local geomorphology and tectonics of the area and the magnitude of the event. The results are compiled in Table 2, listing the causative faults for the events felt in the Naples area, the relative parameters, and the data sources. We also provide comments and additional details specific for the single faults. In general, since most of the earthquakes occurred in historical times, no robust data are available to determine the causative fault, the fault geometry, and mechanism (e.g., focal mechanism solutions). For this reason there are several cases where the association of event/fault and fault/parameters is not straightforward and then we discriminate based on our expertise. In case of inconsistency of the published data, we provide the alternative solutions always based on the geological and tectonic setting of the area. When this is the case, a single earthquake might be associated with more than one tectonic structure. Among these, the 30 March 1627 earthquake in the Gargano area is attributed to three faults with different locations and kinematics by different authors, i.e., the Apricena fault (code 7 in Table 2), the Apricena-Sannicandro fault (code 8 in Table 2), and the San Severo fault (code 14 in Table 2).

The list in Table 2 also includes multiple events associated with the same causative fault. This is the case for the 8 September 1694 and the 23 November 1980 earthquakes that could have nucleated on the same seismogenic source. This source is here distinguished in Pescopagano 1 and Pescopagano 2 faults (codes 38 and 41c in Table 2, respectively) since it ruptured differently during the two seismic events. In particular, the Pescopagano 1 fault, activated in 1694 as a single segment with greater dimensions (i.e., W and L parameters in Table 2), produced a larger magnitude event (M6.8), with respect to the one in 1980 (M6.3). We have also taken into account the fault systems, both as a single tectonic structure that generates large events and as that consisting of multiple active segments that generate individual seismic events. One in the list is the Monte Marzano Fault System (code 41 in Table 2), characterized by different rupture episodes that nucleated along three different fault segments during the 1980 earthquake sequence. Except for the antithetic segment (the Pescopagano 2 fault, code 41c in Table 2), the other two (the Colliano fault code 41a and the San Gregorio fault code 41b in Table 2) are part of the great fault system with an assigned total length of 37 km (adding the single segment extensions).

A distinct set of faults is compiled in Table 3. It includes the faults from *Cinque et al.* [2000] lacking of earthquake data but supposed to be seismically active and close to the urban area of Naples (Figure 1). These faults are thus potentially hazardous even for low-magnitude events. No historical or recent earthquake is assigned to any of these faults. In general, the faults in Table 3 show a greater length; therefore, they are possibly able to produce larger-magnitude earthquake and their hazard might be higher. In fact, we are aware that major magnitude events, larger than those in Table 2, may be produced by the faults here considered, generating also different rupture dynamics. In order to take this into account, we include the longer Piana del Volturno fault (code b) and Maddaloni-Valle Caudina fault (code e) although already in Table 2, differently named Cassino 2 fault (code 26) and Valle Caudina fault (code 32) and parameters.

Finally, based on our selection, the seismogenic potential of Naples and its surroundings is represented by 59 faults associated with seismic events occurring in historical and recent time (Table 2) and 14 faults without any earthquake date associated (Table 3). The whole set of faults is mapped in Figure 2. The details on the data application of Tables 2 and 3 in the synthetic simulation of the earthquake catalogs are provided in section 3.1.4.

3. Methodology and Application

Different from the frequentist approach, in a Bayesian perspective, there is not a true value for the variables of interest, but they are represented by a probability density function (pdf). The Bayesian inference is the instrument used to best estimate the parameters of that pdf. Practically, this is accomplished by merging a prior model for the variables with a set of past observations (y) in order to maximize the probability of having observed those data with that prior model in mind. The prior model is defined as $[\vec{\Theta}]_{prior}$, where $\vec{\Theta}$ is the vector

Table 2. The 59 Active Faults Associated to the Seismic Events in Table 1[a]

Code	Fault Name	Lat1	Lon1	Lat2	Lon2	Lat3	Lon3	*L*	*W*	Strike	Dip	Rake	Min Depth	Max Depth	Earthquake (MM-DD-YY)	M_w	Mean Recurrence Time	SD Recurrence Time	Note
1	Valnerina	42.643	13.189	42.718	13.104			11.0	10.0	160	50–60	270	1.0	8.0	9-19-1979	5.9			*Deschamps et al.* [1984] and *Galli et al.* [2005].
2	Maiella-Porrara	42.150	14.040	41.920	14.100			26.0	15.0	160–170	60	270	1.0	13.0	11-3-1706	6.8			1160 (T-bar) RC in *Akinci et al.* [2009].
3	Fucino Basin	42.089	13.564	41.901	13.795			28.0	15.5	135	60	270	1.5	14.9	13-1-1915	7.0	(1400–2600) 2000^	±600	^based on paleoseismology; value for the past 10,000 years
4	Palena	42.010	14.080	41.990	14.130			5.0	8.0	110–120	60–70	270	8.0	15.0	08-25-1905	5.2			Active faults from this study.
5	Gargano	41.856	15.823	41.884	16.046			19.0	10.0	78–122	40–50	112	5.0	13.0	05-31-1646	6.6			Active faults from this study.
6	Sora_2	41.833	13.548	41.705	13.750			20.0	12.0	130	60–80	270	1.0	12.0	7-24-1654	6.3			Two possible faults for the same earthquake: Sora_2 (n. 6) from the Report of Firb Fumo Project and Sora_1 (n. 11) from *Galadini et al.* [2001].
7	Apricena	41.813	15.232	41.753	15.521			25.0	21.0	285	60–70	270	1.0	20.0	3-30-1627	6.7			Event assigned to three different tectonic structures: Apricena (n. 7) [*Patacca and Scandone*, 2004], Apricena-Sannicandro (n. 8) and San Severo (n. 14). The uncertainties of the parameters are high for all three solutions provided.
8	Apricena-Sannicandro	41.780	15.240	41.832	15.566			26.0	15.0	65–85	80	280	1.0	20.0	3-30-1627	6.7			As for fault n. 7. Reference for Apricena-Sannicandro fault is *Salvi et al.* [1999].
9	Candelaro	41.769	15.405	41.557	15.735			28.0	12.0	310	80	240	1.0	12.0	12-6-1875 2-21-1841	5.3 min 6.0 max			The 1841 and 1875 earthquakes could be assigned to Candelaro (n. 9) and/or San Marco in Lamis (n. 13) faults.
10	Barrea	41.750	14.017	41.693	14.051			10.0	7.5	152	50	264	5.0	10.7	5-7-1984	5.9	(270–2700) 1485*	±1215	*Mean recurrence time from slip rate and average displacement.
11	Sora_1	41.733	13.593	41.665	13.765			16.0	12.0	116	65	270	1.0	12.0	7-24-1654	6.3			As for fault n.6.
12	Monti della Meta	41.714	13.786	41.689	13.843			6.5	5.7	127	60–80	270	1.0	10.0	12-6-1874	5.5			Parameters from *Akinci et al.* [2010] and from *DISS WG* [2010].
13	San Marco in Lamis	41.700	15.590	41.690	15.840			21.0	12.0	85–95	80	215	0.0	12.0	12-6-1875 2-21-1841	5.3 min 6.0 max			As for fault n. 9.
14	San Severo	41.676	15.151	41.688	15.557			34.0	15.0	266	80	215	6.0	21.0	3-30-1627	6.7			As for fault n.7. Reference for San Severo fault is from *DISS WG* [2010].
15	Monti del Matese	41.600	14.209	41.554	14.250			6.0	9.8	146	50–60	270	2.0	10.0	6-6-1882	5.3			Active fault from this study.
16	Boiano Basin	41.580	14.260	41.440	14.540			30.0	13.8	304	55	270	1.0	12.3	7-26-1805	6.6	(970–9,700) 5,335*	±4,365	*data from slip rate and average displacement.
17	Cassino_1	41.547	13.667	41.481	13.812			14.0	8.5	121	60–80	270	2.0	10.0	7-21-1806	5.1			Fault parameters partially from the Report of Firb Fumo Project and from this study.
18	Matese	41.547	14.678	41.507	14.745			7.0	10.3	130	70–80	290	5.0	15.0	10-4-1913	5.4			Active faults from this study.
19	Aquae Iuliae	41.520	14.090	41.410	14.270			22.0	13.0	125	65	270	1.0	12.8	9-9-1349	6.6	min 1,500^		^based on paleoseismology [*Galli and Naso*, 2009].
20	Cerignola_2	41.365	15.705	41.231	15.898			20.0	18.3	130	50–60	270	5.0	20.0	3-20-1731	6.5			Two possible faults: Cerignola_2 (n. 20) from DPC Report and *Del Gaudio et al.* [2007], and Cerignola 1 (n. 24) from *DISS WG* [2010].
21	Sannio	41.352	14.314	41.279	14.533			20.0	9.2	114	60	270	2.0	10.0	9-4-1293	5.8			Fault parameters partially from *Galadini et al.* [2001] and this study.
22	Mattinatella	41.350	16.016	41.350	16.099			7–9	6.3	270	80	180	13.0	19.0	6-19-1975	5.2			Fault parameters partially from *Di Bucci et al.* [2007], *DISS WG* [2010], and this study.
23	Sannio_2	41.324	14.521	41.145	14.869			35.0	13.5	124	55	270	1.5	10.0	6-5-1688	7.0			Two possible faults for the same earthquake: Sannio_2 (n. 23) from *Di Bucci et al.* [2005] and Sannio_1 (n. 25) from Traiano Project (unpublished).
24	Cerignola_1	41.270	15.680	41.270	15.910			18.6	11.3	269	80	180	11.3	22.1	3-20-1731	6.5	1,200–6,000*	3,600 ± 2,400	*Inferred from slip rate and average displacement. As for fault n. 20.
25	Sannio_1	41.265	14.344	41.136	14.702			32.0	12.7	296	60	270	1.0	12.0	6-5-1688	7.0			As for fault n. 23.
26	Cassino_2	41.235	14.164	41.199	14.203			5.0	6.9	140	60	270	4.0	10.0	28-8-1720	4.8			Fault parameters partially from *Galadini et al.* [2001] and this study.
27	Cerreto	41.225	14.636	41.216	14.695			6.0	13.0	101	50–60	270	1.0	10.0	5-25-1927	5.0			Fault parameters partially from *Cinque et al.* [2000] and this study. This fault is the same structure of GNDT compilation well known as Benevento fault (n. 58), but it has a new location in this study to better fit with the 1927 earthquake.
28	Ariano Irpino	41.190	14.890	41.160	15.230			30.0	14.9	277	70	230	11.0	25.0	12-5-1456	7.2	2,000–20,000*	11,000 ± 9,000	*Inferred from slip rate and average displacement.
29	Irpinia-Ufita_1	41.152	15.034	41.002	15.205			22.0	17.0	140	50–60	270	1.0	15.0	11-29-1732	6.6			Two possible faults: Irpinia-Ufita_1 (n. 29) from *Galadini et al.* [2001] and Irpinia-Ufita_2 (n. 31) from *DISS WG* [2010]. Location and fault parameters not very well constrained.
30	Beneventano-Irpinia	41.101	14.858	40.990	14.997			18.0	10.4	136 ± 20	55 ± 15	270	4.0	10.0	3-14-1702	6.5			Fault parameters from Traiano Project (unpublished).
31	Irpinia-Ufita_2	41.034	14.949	41.015	15.257			25.6	14.5	275	64	237	1.5	14.5	11-29-1732	6.6			Two possible faults for the same earthquake: Irpinia-Ufita_2 (n. 31) from *DISS WG* [2010]; and Irpinia-Ufita_1 (n. 29) from *Galadini et al.* [2001]. Location and fault parameters not very well constrained
32	Valle Caudina	41.032	14.515	41.036	14.586			7.0	9.2	84	60	270	2.0	10.0	5-4-1903	4.7			Length and location from *Cinque et al.* [2000] (Napoli fault, n. 28), the other parameters from this study.
33	Irpinia	41.026	15.292	40.972	15.664			32.0	16.5	280	65	213	2.0	17.0	7-23-1930	6.6			Fault parameters from *Pino et al.* [2008] and the location is from *DISS WG* [2010], with the name Bisacce fault.

Table 2. (continued)

Code	Fault Name	Lat1	Lon1	Lat2	Lon2	Lat3	Lon3	*L*	*W*	Strike	Dip	Rake	Min Depth	Max Depth	Earthquake (MM-DD-YY)	M_w	Mean Recurrence Time	SD Recurrence Time	Note
34	Avella	40.993	14.549	40.978	14.633	7.0	13.0	103	50–60	270	1.0	10.0	02	14	1,981	4.9			The fault parameters have been inferred based on the M_w 4,9. From *Cinque et al.* [2000] and *Galadini et al.* [2001]; the Avella fault is about 15 km long.
35	Beneventano	40.950	14.790	40.940	14.850	5.0	9.5	290	70	270	2.0	8.0	03	14	1905	4.9			Active faults from this study.
36	Mattina-Atella	40.946	15.403	40.859	15.603	20.0	11.0	120	50–60	270	1.0	10.4	09	08	1,694	6.8			Two possible faults for the same event: Mattina Atella (n. 36) from *Galli et al.* [2006]; and Pescopagano_1 (n. 38) from *DISS WG* [2010]. This fault, or a portion, could be responsible for the 1980 event at 40 s (M_w 6,3). The parameters of the Mattina-Avella are similar to those to Pescopagano_2 (n. 40), except for the length. The latter is greater in accordance with the magnitude.
37	Melfi	40.940	15.560	40.940	15.760			17.2	11.0	269	80	180	12.0	22.8	8-14-1851	6.4	1,320–6,600*	3,690 ± 2,640	*Inferred from slip rate and displacement.
38	Pescopagano 1	40.923	15.250	40.817	15.458			20.0	10.0	124	70	270	1.0	10.4	9-8-1694	6.8	286.0		As for fault n. 36.
39	Irpinia-Basilicata	40.917	15.315	40.896	15.420			10.0	17.0	285	60–80	250	2.0	18.0	6-7-1910	5.7			The fault parameters are from *DISS WG* [2010].
40	Napoli	40.863	14.227	40.878	14.287			5.0	6.9	58	60	270	2.0	8.0	6-5-1575	4.9			Length and location from *Cinque et al.* [2000] (Napoli fault, n. 16), other parameters from this study.
41	Monte Marzano fault system	40.850	15.140	40.620	15.500			37.0	15.0	310	60	270	1.0	14.0	11-23-1980	6.9	1,470–2,245^	2,150, 1,858 ± 388	^Based on paleoseismology. Value for the past 10,000 years (based on five events). For the 1980 event (at 0 s and 20 s) the authors give a single tectonic structure given by the union of event at 0 and 20 s.
41a	Colliano	40.850	15.140	40.680	15.380			28.0	15.0	310	60	270	1.0	14.0	11-23-1980 (0 s)	6.9			Fault of 1980 earthquake at 0 s.
41b	San Gregorio	40.670	15.410	40.620	15.500			9.0	15.0	300	60	270	1.0	14.0	11-23-1980 (20 s)	6.9			Fault of 1980 earthquake at 20 s.
41c	Pescopagano_2	40.900	15.290	40.820	15.440			15.0	10.0	124	70	270	1.0	10.4	11-23-1980 (40 s)	6.3			Fault of 1980 earthquake at 40 s.
42	Caposele	40.846	15.141	40.757	15.240			11.0	8.0	310	60	270	1.0	14.0	4-9-1853	5.6			The authors take into consideration the northern portion of the fault of 1980 event although the fault parameters remain rather uncertain.
43	Salernitano	40.793	14.682	40.794	14.745			5.0	6.9	95	60	270	2.0	8.0	4-27-1930	4.8			Length and location from *Cinque et al.* [2000] (Napoli fault, n. 34), the other parameters from this study.
44	Vallo di Diano	40.590	15.414	40.570	15.500	40.543	15.549	13.0	11.7	108–122	70	275	1.0	12.0	8-19-1561	6.8	1.6 ky		The fault parameters are from *Galli et al.* [2006], with the name Caggiano fault.
45	Campomaggiore_1	40.546	16.177	40.541	16.247			6.0	6.2	95	90	175	15.0	20.0	8-8-1846	5.2			Active faults from this study. Two possible active tectonic structures but with different strike: Campomaggiore_1 (n. 45) and Campomaggiore_2 (n. 46). Some fault parameters have been derived from *DISS WG* [2010], and *Galadini et al.* [2001]
46	Campomaggiore_2	40.540	16.169	40.514	16.232			6.0	5.3	118	70	250	15.0	20.0	8-8-1846	5.2			As for fault n. 45.
47	Basilicata	40.518	15.590	40.440	15.651			10.0	12.0	320	65	270	1.0	12.0	2-1-1826	5.8			The fault parameters are from *Moro et al.* [2007].
48	Manduria	40.497	17.650	40.474	17.822			15.0	18.3	100	80	280	2.0	20.0	10-26-1826	5.4			Active faults from this study. The authors are skeptical about the likely shaking in Naples for this event being located far away from the study area.
49	Val d'Agri_2	40.422	15.700	40.344	15.751	40.310	15.810	23.0	13.5	316.0	60	270	1.0	12.7	12-16-1857	7.0			Two possible active tectonic structures: Val d'Agri_2 (n. 49) from *DISS WG* [2010]; and Val d'Agri_1 (n. 50) from *Benedetti et al.* [1998]. The authors choose the SW dipping fault because it is more favorable for shaking in Naples.
50	Val d'Agri_1	40.410	15.740	40.340	15.850	40.320	15.960	34.0	12.0	308–287	60	270	1.0	14.0	12-16-1857	7.0			As for fault n. 49.
51	Basilicata meridionale	40.166	15.907	40.147	15.952	40.096	15.970	20.0	9.2	137–170	60	270	2.0	10.0	11-20-1836	6.0			Fault parameters from this study. Location from *Michetti et al.* [2000].
52	Policastro	40.041	15.630	39.940	15.500			15.0	9.0	40	60	270	1.0	15.0	3-21-1982	5.4			
53	Basso Ionio	39.924	18.798	39.730	19.226			40.0	61.0	123	30–40	90	5.0	40.0	2-20-1743	7.0			Fault parameters from *Galli and Naso* [2008] and *Armigliato et al.* [2007].
54	Catanzaro	38.939	16.385	38.917	16.526			12.0	8.3	280	70–80	280	2.0	10.0	8-2-1821	5.1			Active faults from this study. The location is from *Galadini et al.* [2001] (Lamezia-Catanzaro fault n. 100) and *Galadini et al.* [2000] (fault n. 104).
55	Graben Catanzaro	38.859	16.367	38.769	16.564			20.0	19.8	120	65 ± 10	229 ± 12	2.0	20 ± 5	3-28-1783	6.9			Location from *Galadini et al.* [2001]; but the parameters are from *Sirovich and Pettenati* [2007]
56	Capo Vaticano	38.671	15.880	38.750	16.100			30.0	20.0	245	80	270	1.0	19.6	6-6-1777	6.4	ca. 1,000''		Active faults from this study. ''The repeat time is similar to the Coccorino fault [*Cucci and Tertulliani*, 2010] located nearby. Although the seismic event is located at sea, the fault is on the coast. The fault parameters are not robust. The M_w magnitude of the event is derived from the fault model.

[a]Each fault has an identification code, and it is mapped with red color in Figure 2. Legend: Lat: latitude (deg); Lon: longitude (deg); L: lenght (km); W: width (km); M_w: moment magnitude; sd: standard deviation.

Table 3. The 14 Faults Considered Active Nearby the City of Naples Although No Seismic Event Is Associated[a]

Code	Fault Name	Lat1	Lon1	Lat2	Lon2	Lat3	Lon3	*L*	*W*	Strike	Dip	Rake	Min Depth	Max Depth	Note
a	Monte Massico	41.200	14.030	41.120	13.910			10.0	13.0	48	60	270	1.0	10.0	n. 12 in *Cinque et al.* [2000].
b	Piana del Volturno	41.180	14.040	41.150	14.210			34.0	13.0	109–140	60	270	1.0	10.0	n. 13 in *Cinque et al.* [2000]. A portion of this structure is associated with the 1720 earthquake (Cassino_2 fault, n. 26 in Table 2).
c	Mondragone	41.140	13.830	41.130	13.910			6.0	13.0	108	60	270	1.0	10.0	n. 11 in *Cinque et al.* [2000].
d	Monte Taburno	41.130	14.520	41.070	14.590	41.070	14.680	9.0	13.0	137–100	60	270	1.0	10.0	n. 27 in *Cinque et al.* [2000]; F.431 Caserta Est 1:50.000 ISPRA.
e	Maddaloni-Valle Caudina	41.020	14.400	41.040	14.680			20.0	13.0	84	60	270	1.0	10.0	n. 28 in *Cinque et al.* [2000]. A portion of this structure is associated with the 1981 event (Caudina fault, n. 32 in Table 2).
f	Cancello	40.990	14.320	40.990	14.480	40.970	14.540	9.0	13.0	95	60	270	1.0	10.0	n. 14 in *Cinque et al.* [2000].
g	Monti di Sarno	40.850	14.560	40.800	14.650			9.0	13.0	140	60	270	1.0	10.0	n. 33 in *Cinque et al.* [2000]; and *Franza* [2006].
h	North Monti Lattari	40.740	14.470	40.730	14.760			12.0	13.0	93	60	270	1.0	10.0	n. 35 in *Cinque et al.* [2000]; and *Vitale* [2006].
i	Castellammare	40.720	14.530	40.670	14.410			5.0	13.0	58	60	270	1.0	10.0	n. 20 in *Cinque et al.* [2000].
j	Vico Equense	40.670	14.410	40.600	14.270			15.0	13.0	58	60	270	1.0	10.0	n. 19 in *Cinque et al.* [2000].
k	S. Vito	40.640	15.020	40.590	15.090			8.0	13.0	135	60	270	1.0	10.0	n. 37 in *Cinque et al.* [2000]; and *Vitale* [2006].
l	Ponte Barizzo	40.560	14.950	40.460	15.040			10.0	13.0	150	60	270	1.0	10.0	n. 38 in *Cinque et al.* [2000].
m	P. delle Olive	40.560	15.050	40.540	14.960			7.0	13.0	68	60	270	1.0	10.0	n. 39 in *Cinque et al.* [2000].
n	Golfo di Salerno	40.550	14.300	40.640	14.810			48.0	13.0	78	60	270	1.0	10.0	n. 36 in *Cinque et al.* [2000].

[a]Each fault has an identification code and it is mapped with green color in Figure 2.

Journal of Geophysical Research: Solid Earth

10.1002/2016JB013507

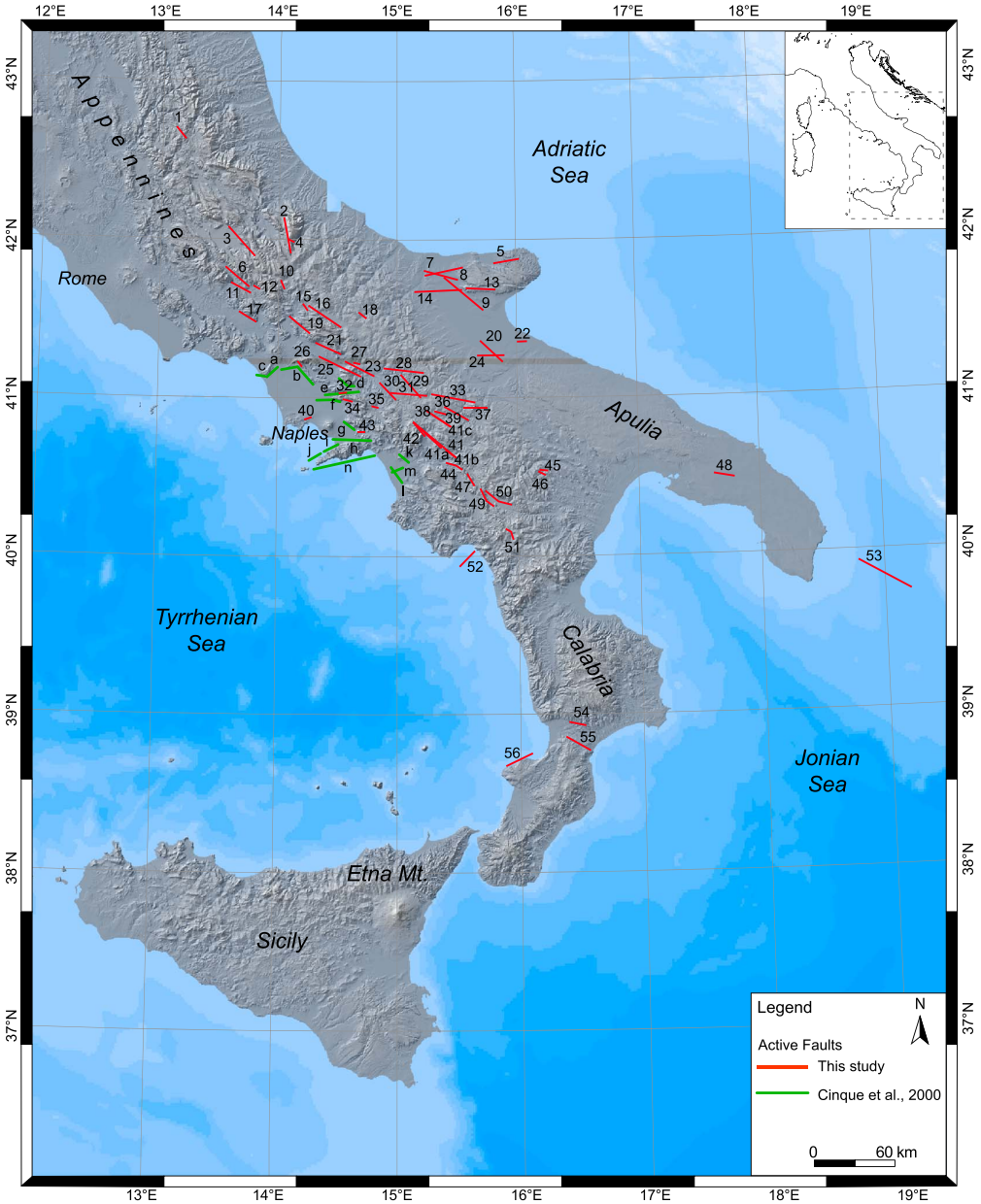

Figure 2. Map of the seismogenic faults listed in Table 2 (red color lines) and in Table 3 (green color lines). These faults are coded as in Tables 2 and 3 where the parameters are listed.

of the variables, and the square brackets denote a pdf. The output of Bayesian inference is thus a posterior distribution ($[\vec{\Theta}|y]$) for the variables of the model. The practical way used for combining prior distribution and data is the Bayes theorem:

$$[\vec{\Theta}|y] = \frac{[\vec{\Theta}_{\text{prior}}][y|\vec{\Theta}]}{[y]}, \tag{1}$$

where $[y|\vec{\Theta}]$ is the so-called likelihood function (representing the probability of observing data y given parameters $\vec{\Theta}$), and $[y]$ is a normalizing factor accounting for the total probability of observing the data y. With Bayesian inference the uncertainty of $\vec{\Theta}$ is also provided. In particular, while the mean of the posterior pdf

represents a kind of best estimate given the intrinsic randomness of the process (aleatory uncertainty), its variance is an estimation of the epistemic uncertainty related to the limited knowledge of the process; see *Gelman et al.* [2000] for more details.

We apply a methodology similar to the one adopted in *Selva and Sandri* [2013]. The probabilistic hazard consists of assessing, given a certain location z and an exposure time ΔT, the probability that a certain value of shaking is exceeded, through the quantification of the seismic-hazard curve. The intensity measurement is the peak ground acceleration (PGA). Following *Marzocchi et al.* [2015], this probability is interpreted as the long-term frequency of exceedance that could be measured after a large number of equivalent exposure time windows ΔT. The epistemic uncertainty on quantifying this frequency is then represented through a probability density function (pdf). The assessment of such a pdf is here performed following a Bayesian inference scheme.

First, we focus on a generic target location, which we generically call z (we underline that such methodology may be applied to a set of different locations). We consider a discrete set of K PGA values in increasing order:

$$\epsilon_1 < \epsilon_2 < \cdots < \epsilon_K \tag{2}$$

where $\epsilon_1, \ldots, \epsilon_K$ are the PGA threshold levels. For each of these values, the logical variable O_i is true if there exists at least one PGA value larger than or equal to ϵ_i in the time window ΔT. $[\Theta_i] = p(O_i)$ is the probability of O_i being true. The probabilities $[\Theta_i]$, with $i = 1, \ldots, K$ are not independent; in fact, O_i being true implies that O_j is true if $j \leq i$. Following *Marzocchi et al.* [2008] and *Selva and Sandri* [2013] it is possible to develop a full description of the hazard curve, exploring the properties of the dependency of $[\Theta_i]$; writing $[\Theta_{i+1}]$ in terms of $[\Theta_i]$,

$$p(O_{i+1}) = p(O_{i+1}|O_i)p(O_i) + p(O_{i+1}|\bar{O}_i)p(\bar{O}_i) \tag{3}$$

where $\bar{O}_i$ corresponds to the case in which ϵ_i is not exceeded. In equation (3), $p(O_{i+1}|\bar{O}_i)$ is always 0 since the probability to exceed ϵ_{i+1} is null if ϵ_i has not exceeded. This leads to rewrite equation (3) as

$$[\vec{\Theta}_{i+1}] = \vec{\Theta}'_{i+1}\vec{\Theta}_i \tag{4}$$

where $\vec{\Theta}'_{i+1}$ is the conditional probability of O_{i+1} given O_i. By iteration, equation (4) can be rewritten as

$$[\vec{\Theta}_i] = [\vec{\Theta}_1]\prod_{j=2}^{i}[\vec{\Theta}'_j] \tag{5}$$

where $[\vec{\Theta}_i]$ is the probability of O_i being true and $[\vec{\Theta}'_j]$ is the conditional probability of $[\vec{\Theta}_j]$ given $[\vec{\Theta}_{j-1}]$.

In the framework of Bayesian inference, the prior model represents our present reference states of knowledge of the process, which is then updated by the available information of past shaking (i.e., the likelihood) by means of Bayesian rules, to obtain the posterior probability. In this context, the prior model is represented by the PSHA assessment which can be updated by the shaking data on past earthquakes in the area.

The following sections focus on the description of the prior model, the likelihood, and the posterior distribution.

3.1. The Prior Model

The prior hazard model is evaluated by the probabilistic analysis of all possible seismic sources in the area around Naples. Several alternative models are adopted to parameterize the earthquake occurrence with the goal to analyze and quantify the variability in earthquake modeling. As mentioned in section 1, our uncertainty analysis focuses on the modeling of the earthquake occurrence and neglects the contribution of the GMPEs, which is left for future studies. The final result is presented in terms of median and percentiles (e.g., *Stucchi et al.* [2011], for PSHA in Italy). In this work, we apply different models to define these earthquake distributions. These models are based on different hypotheses on the seismogenic process. In this way, we provide a much wider perspective of the problem, covering the possibility that a single model is not able to entirely explain the earthquake occurrence. The statistical modeling of the earthquake occurrence has been calculated adopting either the time-dependent earthquake models or the Poisson model. The inclusion of the time-dependent models is done considering both the short-term earthquake clustering of the seismicity—which could be relevant in medium-term hazard analysis, and the long-term behavior—which

could play a role in long-term hazard assessment. The Poisson model has been included as a benchmark, because it is still widely used in the long-term seismic hazard analysis, as, e.g., in the Italian seismic hazard map [*Stucchi et al.*, 2011]. In total, we use five different models. For all of them, the time and space dependency among earthquakes is included into the hazard analysis via Monte Carlo simulations. In four out of five of the adopted models, the aftershock sequences are included, by using the Epidemic Type Aftershock Sequence (ETAS) [*Ogata*, 1988] model. The difference among the four time-dependent models is in the definition of the background, parameterized in one case using a Poisson model, and in the remaining three cases using the information on the statistical occurrence of known faults in the areas surrounding Naples, using the Brownian Passage Time distribution [*Matthews et al.*, 2002].

We evaluate the impact of the hazard for three exposure times: 5 years, 10 years, and 50 years. The statistical models describe the earthquake occurrence in terms of time, space, and magnitude. In each simulation and for each statistical model, we use the real instrumental catalog as input, updated at 11 April 2016, so each simulation takes into consideration the recent seismic history. In addition, for models that include fault data, the simulations are conditioned to the time of the last earthquake occurred on each fault. In this way, we have included the most recent seismic history in the earthquake modeling. The spatial distribution of the background activity is calculated by a spatial smoothing of declustered past seismicity; while the occurrence on fault is only considered for the Brownian Passage Time models (see below for details). To parameterize the size distribution, we adopt the Gutenberg-Richter (G-R) relation [*Gutenberg and Richter*, 1944] to all spatial scales and a wide range of earthquake magnitudes.

Once the earthquake probabilistic distribution is set up, the prior distribution of hazard assessment is evaluated by using Monte Carlo catalog simulations, where each catalog is intended as a representation of the real seismicity. To define the expected ground shaking, the GMPE is applied.

3.1.1. Monte Carlo Simulation

Following *Beauval et al.* [2006] and *Faenza et al.* [2007], the evaluation of the probability of nonexceedance of a particular ground motion value during the exposure time is evaluated using Monte Carlo techniques. This use of synthetic catalogs is another way to calculate the probabilistic seismic hazard analysis [*Rosenblueth*, 1964; *Musson*, 1999; *Smith*, 2003; *Giardini et al.*, 2004].

In the conventional approach, the hazard at a site is evaluated by considering the ground motion from all possible damaging earthquakes that can occur in a region. In fact, in a time-independent study, the annual rate is sufficient to express earthquake occurrence. In this case, the seismic hazard can be computed in terms of annual rates of exceedance of selected acceleration levels ($A^\star$) at the site of interest, using the relation [*Ang and Tang*, 1975]: $P(A \geq A^\star) = 1 - \exp(-\lambda t)$, where λ is the annual rate of the target event and t is the time of interest. Using a Taylor series expansion for small λt and truncated at the first term, the exceedance probability becomes approximated equal to the annual rate λ times t. Considering a time-dependent earthquake occurrence, the seismic hazard cannot be expressed in term of annual rate of earthquake occurrence any longer. In *Beauval et al.* [2006] and *Faenza et al.* [2007], the Monte Carlo techniques are applied to the study of the temporal behavior of earthquakes, in particular, to estimate the impact of the Poisson hypothesis on seismic hazard versus a time-dependent behavior of seismicity, either in the short term or long term. This approach is further utilized in the present study. For the evaluation of the hazard, a sufficient large number of synthetic catalogs (N) of time duration t is generated. For each catalog, a set of ground motions is evaluated. The probability of nonexceedance of a level $A^\star$ of ground motion at a specific site in the time t is computed by counting the intervals in which $A^\star$ did not occur

$$P(A^\star; t) = \lim_{N\to\infty} \frac{1}{N} \sum_{i=1}^{N} H(A^\star - A_{\max,i}) \tag{6}$$

where N is the number of catalogs of time duration t; H is the Heaviside function, and $A_{\max,i}$ is the maximum ground motion value that occurred at the site of interest during the ith catalog of time duration t. The complement of $P(A^\star; t)$, i.e., $1 - P(A^\star; t)$, is the probability that $A^\star$ is exceeded at least once in the time period t. An alternative way to estimate the probability of nonexceedance is to consider directly the empirical density function of the maximum acceleration values $A_{\max,i}$. Each probability of nonexceedance is identical to the corresponding percentile of this distribution (further details in *Beauval et al.* [2006] and *Faenza et al.* [2007]).

3.1.2. The ETAS Catalogs

The inclusion of the aftershock activity into the analysis is done through the ETAS model—Epidemic Type Aftershock Sequence. The ETAS model is a stochastic marked point process for the representation of the

occurrence of earthquakes of size larger than or equal to a threshold magnitude, in a given region and period of time [*Ogata*, 1988]. Among the few spatiotemporal models proposed in literature, the ETAS model is by far the most frequently applied, and in some cases, it has been defined as the best way to describe short-term seismicity [*Console et al.*, 2007; *Zhuang et al.*, 2011, 2013] since its formulation in 1988 by *Ogata* [1988]. It assumes that there is no difference in triggering seismicity among foreshocks, main shocks, and aftershocks, and each event triggers its own offspring independently according to some probability rules. It works by considering the seismicity as the superposition of seismicity induced by previous events on the background. The hazard rate of the ETAS model is defined as

$$\lambda(t,r) = \mu\, u(r) + K_0 \sum_{t_i<t} \frac{10^{(\alpha*(m_i-m_0)}}{(t-t_i+c)^p} \frac{q-1}{\pi D_i^2} \left(1 + \frac{|\vec{x}-\vec{x}_i|^2}{D_i^2}\right)^{-q} \tag{7}$$

where μ is the background rate (unit of time) of the seismicity and represents the tectonic loading, while the cascade of aftershocks is described by the empirical Omori-Utsu law [*Utsu et al.*, 1995], $(t+c)^{-p}$, with t being the time from the occurrence of the main shock. The probability density function of the triggered events is parameterized as a long tail inverse power law with a magnitude-dependent length scale $D_i = d_0 10^{\gamma m_i}$. The parameter α is a measure of the efficiency of a shock in generating aftershock activity and relative to its magnitude; K_0 represents the productivity of an event of threshold magnitude m_0. A complete description can be found in *Ogata* [1988, 1998].

For the joint inversion of the eight parameters we use the data in the ISIDe database (the Italian Seismological and Parametric Data Base) [*ISIDe Working Group*, 2010] for shallow events (depth $\leq$ 30 km) in the time period 2005–2016 (11 April) for a large area, from the Central Apennines to the Calabrian Arch (Figure 3). This area covers the epicenters of the earthquakes felt in Naples, as analyzed in *Faenza et al.* [2013]. We use $m_0 = 2.9$ for which the data set is complete based on the G-R relation (Figure 3). The fit of the eight parameters of the ETAS model yields: $\mu = 0.1256$ d^{-1}; $p = 1.1071$; $c = 0.0170$ day; $K_0 = 0.0209$; $\alpha = 0.7084$, $q = 2.1996$; $d_0 = 0.3617$; and $\gamma = 0.1947$, according to the procedure of *Zhuang et al.* [2004], where the spatial inhomogeneous background rate and the ETAS parameters are simultaneously estimated based on an iterative procedure. The parameter b of the G-R relation is 1.08 ± 0.03.

We will refer to the catalogs generated by using the ETAS model as the ETAS catalogs. In each instance, events are simulated sequentially: first, the time, then the magnitude, and the epicentral coordinates. The maximum magnitude is set to M_w7.5 following the *Stucchi et al.* [2011] for these areas. We are aware of the problems regarding the definition of the maximum magnitude as deeply analyzed by Zöller and coauthors [*Zöller*, 2013; *Zöller et al.*, 2013]. Tests with maximum magnitude 8.0 have provided similar results.

A Gaussian distribution is used for the spatial smoothing of the background rate, with fixed standard deviation of 20 km, in a grid with 0.05° spacing. To smooth each location of the grid, we use both instrumental and historical catalogs, since the seismicity of the last 11 years could not be representative of the (spatial) distribution of large earthquakes. The historical events are taken from *Grünthal and Wahlström* [2012] catalog, which is assumed to be complete for South Italy since 1650 for $M \geq 5.0$. Each event is weighted by its probability to be a background event: for the instrumental catalog this probability results from the ETAS parameters [*Zhuang et al.*, 2004], while for the historical events this probability is always set to 1; e.g., all the historical events are assumed to be main shocks. The depth of the events is set to 10 km for simplicity. This will not effect the results since the GMPE implemented uses the R_{jb} distance, which is distance to the vertical projection of the fault to the Earth's surface The simulated catalogs are in M_l; to apply the GMPE we first convert M_l in M_w using the regression analysis of *Gasperini et al.* [2013].

3.1.3. The Poisson Catalogs

The Poisson catalogs are defined as the background events of the ETAS catalogs. The Poisson model has only one parameter, the rate parameter, which is the inverse of the mean of the distribution. In this application, we have set the background rate $\mu = 0.1256$ per day according to the ETAS estimations. For the spatial distribution of the background events, we use the same smoothed spatial grid adopted for the ETAS model, which combines the location of the instrumental and historical earthquakes, through a Gaussian filter in a 0.05° spaced grid.

3.1.4. The Brownian Passage Time Catalogs—BPT Catalogs

To account for the inclusion of occurrence of large earthquakes on major faults, we adopt the Brownian Passage Time (BPT hereinafter) distributions [*Matthews et al.*, 2002]. We choose the BPT distribution since it

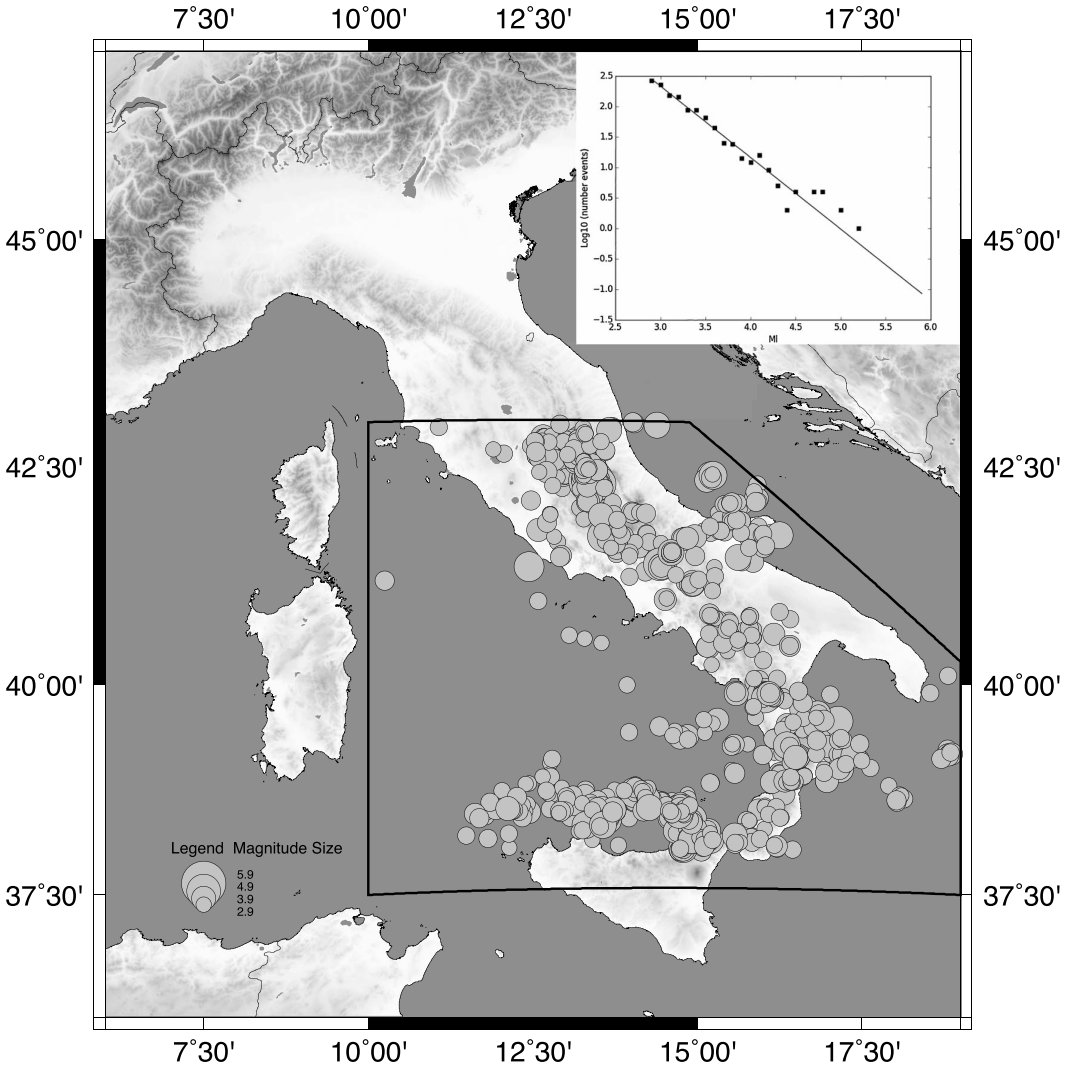

Figure 3. Spatial distribution of the earthquakes in ISIDe, with depth $\leq$ 30 km and minimum magnitude 2.9. Inset: Frequency-Magnitude distribution (points) in the area of interest in the time period 2005–2013, from ISIDe database. The line refers to the G-R law with $b = 1.08$.

is a statistical representation of Reid's elastic rebound theory. BPT distribution has been developed with the dual aim to make a connection between the rebound theory and the real distribution of interevent data, and to build up a physically motivated renewal model for earthquake recurrence. In BPT model, the constant tectonic loading is superimposed by a Brownian perturbation, which makes the stress loading a Brownian relaxation oscillator (BRO). The Brownian perturbation could be interpreted as a physical representation of the fault interactions leading to external perturbations of the stress loading on the fault. In the BRO model, a new earthquake will occur when a state variable (or a set of them) reaches a threshold (X_f), it relaxes the load state to the characteristic ground level (X_0) and begins a new cycle. In the BPT model, the loading of a fault is the composition of two elements: a constant-rate loading component, λt, and a random component, $\epsilon(t) = \sigma W(t)$, as a Brownian motion (where $W(t)$ is a standard Brownian motion and σ is the nonnegative scale parameter). The standard Brownian motion is simply the integration of stationary increments where the distribution of the increments is Gaussian (which might be motivated by central-limit arguments if the perturbations are considered as the sum of many small, independent contributions), with zero mean and constant variance:

$$X(t) = \lambda t + \sigma W(t) \tag{8}$$

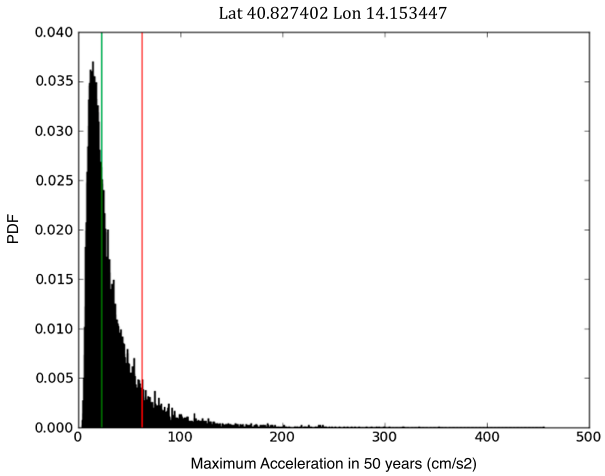

Figure 4. The empirical density function of the $A_{max,i}$ in 50 years based in 20,000 catalogs, for the Poisson catalogs in one site within the dense grid covering the city of Naples. The green line represents the 50th percentile; the red line the 90th percentile at the site.

The BRO model belongs to the family of stochastic renewal processes identified by four parameters: the mean loading (drift) rate (λ); the perturbation rate (σ^2); the ground state (X_0); and the failure state (X_f). The recurrence properties of the BRO (interevent times) are described by a Brownian passage time distribution which is characterized by two parameters: the mean recurrence time (μ) and the aperiodicity (α) of the recurrences which is equivalent to the coefficient of variation ($\alpha = \sigma\mu$).

Tables 2 and 3 list the tectonic structures considered in these simulations. In the case where the mean value is missing, we choose $\mu = 3000$ years. The aperiodicity is the shape parameter of the distribution, because its value changes the width of the distribution. Smaller values of the aperiodicity correspond to a more regular temporal behavior of the sequence, with a nearly symmetric density function where the central value is close to the mean. On the contrary, larger values produce more random occurrence, with a density function skewed to the right and sharply peaked at a value left of the mean [*Matthews et al.*, 2002]. Due to the scarce knowledge of the activity on individual faults, it is not possible to estimate the aperiodicity. Therefore, we decide to work with three distinct values: 0.3, 0.5, and 0.7, in order to range different possibilities in cycling earthquake occurrence. In the simulation, we first simulate the background events and then for each event its own aftershocks sequence. The rate of on-fault events with $M_l \geq 6.5$ is comparable with the one expected from the Poisson rate. For smaller sizes the fault data base is incomplete and the on-fault BPT background events are consequently also not complete, so we added Poisson type events for $M_l < 6.5$. For the spatial distribution of the latter events, we used the same smoothed spatial grid as for the Poisson catalogs. We called these catalogs BPT catalogs; for their generation, we follow the same procedure as before for the ETAS catalogs, modifying only the background events. Specifically, we have generated BPT earthquakes on each single fault, adding some randomness in the magnitude occurrence, by sampling the magnitude from a G-R law, in a range of magnitude of ± 0.5 magnitude units. This is done for each single fault in Tables 2 and 3. In addition, as described in section 2, there are some debated structures. To include this aspect in the hazard, we have generated the synthetic catalogs using the different options in the tables as alternatives. Since we consider the uncertainties of the alternative model, the cumulative fault data set, as described in Tables 2 and 3, changes in each simulation.

3.1.5. Simulations

As target locations we consider the dense grid of 200 m spacing on the municipality of Naples, for a total of 2962 points covering a spatial area of almost 120 km^2. For the calculation of the hazard, a sufficient large number of catalogs (20,000) of 5, 10, and 50 years of duration is generated. For each $M_w \geq 4.0$ earthquake, the peak ground acceleration value at the site of interest is calculated by using the *Akkar and Bommer* [2010] ground motion relation. $M_w = 4.0$ is the threshold magnitude for this ground motion relation. The log(PGA) value was chosen randomly from a Gaussian density function with a standard deviation truncated at three standard deviations. In Figure 4, the density function of maximum acceleration in 50 years for one site is shown

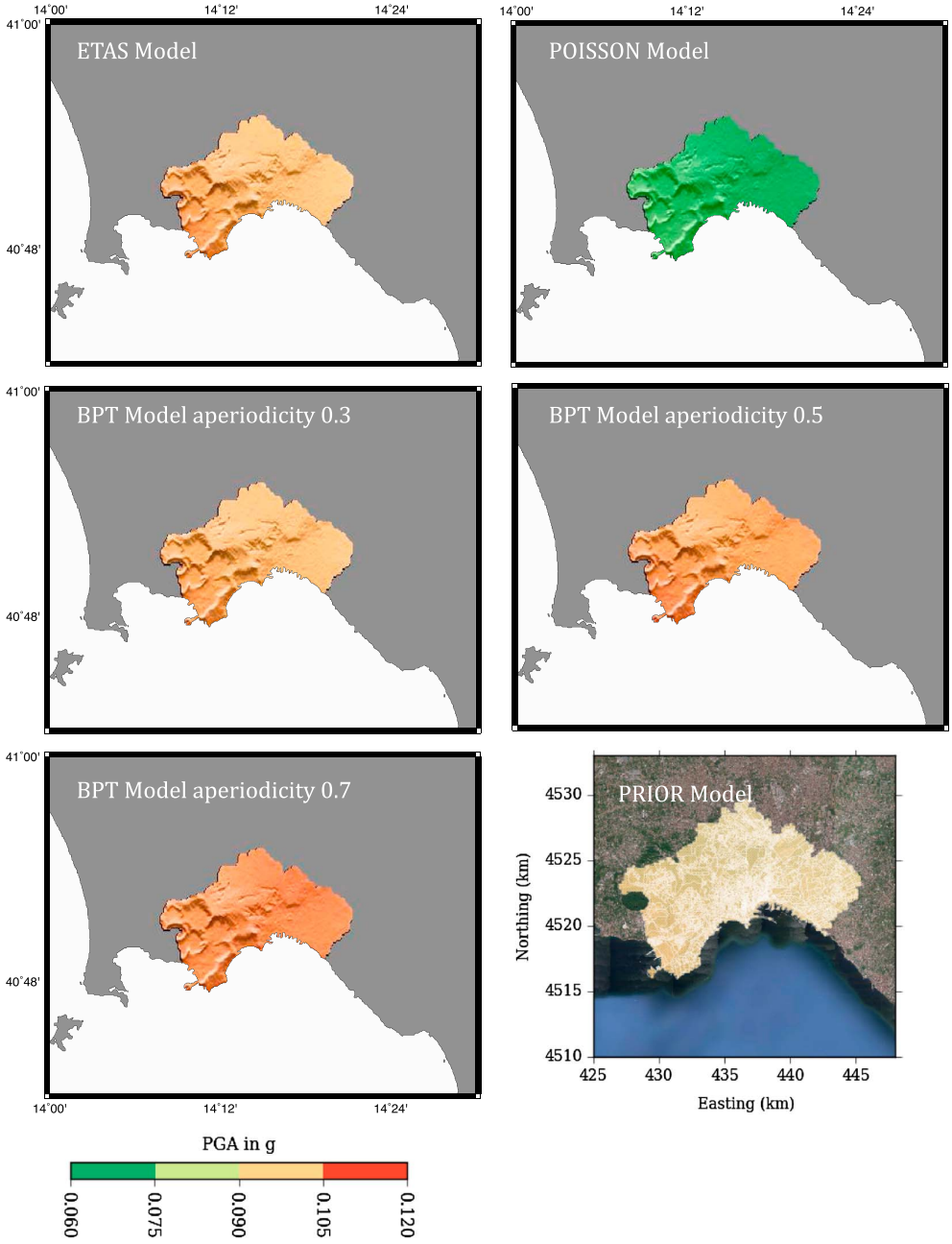

Figure 5. Hazard map as the 10% probability of exceedance in the next 50 years for the ETAS model, the Poisson model, the BPT model with aperiodicity 0.3, 0.5, and 0.7, and the prior model (see details in text) obtain by the ByMur software.

for the Poisson catalogs. The probability of nonexceedance can be deduced directly from this figure, and it corresponds to the percentile of the distribution [*Beauval et al.*, 2006; *Faenza et al.*, 2007]. For instance, 90% of probability of nonexceedance corresponds to the red line and 50% of probability to the green one. Figure 5 shows the a priori model for the Bayesian hazard analysis for exposure time of 50 years. Qualitative similar results are obtained for a time interval of 5 and 10 years (see supporting information). The values of the Poisson model are smaller since the exclusion of the aftershocks activity, confirming that the declustering of the catalog in seismic hazard analysis implies an underestimation of the hazard [*Faenza et al.*, 2007].

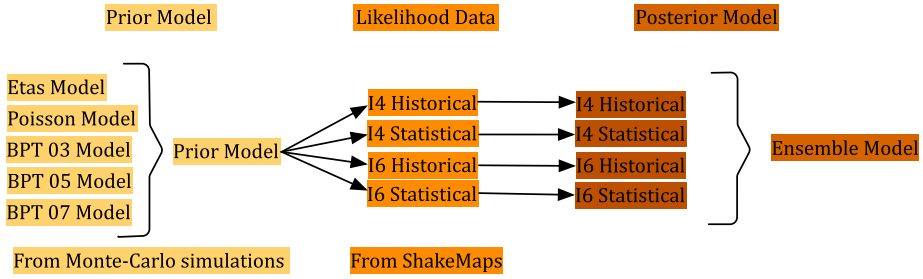

Figure 6. Scheme of the models used to build up the hazard model. The figure shows the models for one exposure time and for rock-type soil; the same structure is implemented for the other exposure time. If the soil amplifications are contemplated in the Monte Carlo simulations and in the ShakeMaps, the amplification factors due to the soil conditions are included.

The results are slightly smaller than those obtained by the seismic hazard map of Italy [*Stucchi et al.*, 2011], in which the area of Naples has a PGA range of 0.150–0.175 of 10% probability of excellence in 50 years. The BPT models with aperiodicity of 0.7 and 0.5 show the highest hazard values in all exposure time. The BPT model with aperiodicity of 0.3 has smaller values compared to the other two BPT models. This could imply that, given a very regular behavior of the occurrence of large events, the faults near Naples are in the cycling phase far from the nucleation of the next event.

These five hazard models are then included in a single model via Beta distribution, to construct the prior model for the Bayesian approach. In detail, for each exposure time ΔT and location z we calculate the probability of exceedance of the hazard for each ϵ_i in equation (2). Equation (5) calculates the conditional probability $[\Theta_i']$ to exceed the hazard value ϵ_i subject to have reached the PGA value ϵ_{i-1}. We obtain five estimations of Θ_i, one for each prior model; and we shape them using Beta distribution that best fit the data:

$$\begin{aligned}[\Theta_1] &= [p(O_1)] = \text{Beta}(\alpha_1, \beta_1) \\ [\Theta_i'] &= [p(O_i|O_{i-1}] = \text{Beta}(\alpha_i, \beta_i).\end{aligned} \tag{9}$$

We use a Beta distribution for the prior pdf as it is appropriate for describing a probability, since its domain is the interval [0, 1].

3.2. The Likelihood

The data used to update the prior distribution are the information on past shaking on Naples. *Faenza et al.* [2013] have analyzed the shaking of Naples using the most up-to-date catalogs and database. They have found completeness in the shaking for two levels of macroseismic intensity, $I \geq 4$ and $I \geq 6$, which correspond to level "felt" and "damage" in the intensity scale, respectively. They also used two distinct methodologies to calculate the completeness. One is based on statistical criteria and the other on historical analysis [*Faenza et al.*, 2013]. For the historical completeness, the temporal threshold is 1500 and 1300 for I_4 and I_6, respectively, while for the statistical one is 1550 and 1420. The details of these calculations are explained in *Faenza et al.* [2013]. We proceed considering these four options independently and merging them at the end of the Bayesian procedure, adopting an ensemble model.

The natural choice for the likelihood function is the binomial distribution, because we use past observations as counts of occurrence or lack of occurrence, successes, or failures, i.e., a Bernoulli trial scheme. The complete time periods of the four likelihoods are divided into chunks of 5, 10, and 50 years, e.g., the three different exposure times, starting from the beginning of the completeness. The assumption substantiating this choice is that past observations are independent trials (which is true within each of the four sets of data based on different completeness methodology and intensity threshold) and can be seen either as a success or a failure. For $i > 1$, we use the following definitions:

1. Trial: a time window in which ϵ_{i-1} is overcome at least once.
2. Success: ϵ_i has been overcome at least once in the Trial time window.
3. Failure: ϵ_i has never been overcome in the Trial time window.

The total number of trials is then the number of time windows in which ϵ_{i-1} is exceeded. For $i = 1$, given the definition of $[\vec{\Theta}_1]$, the success or failure is not conditioned to the occurrence of smaller intensities, so that each

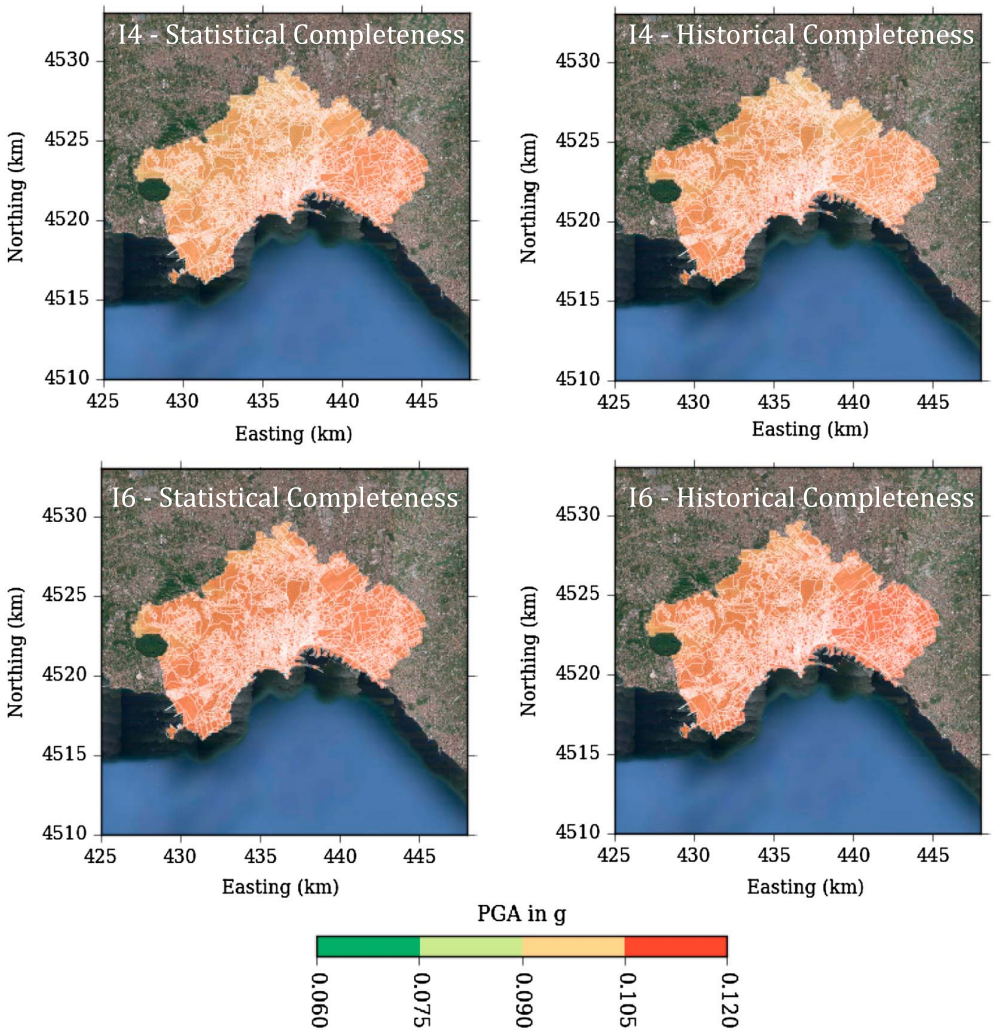

Figure 7. Hazard map as the 10% probability of exceedance in the next 50 years, on the basis of the posterior model using four different likelihood data.

time window is a trial and success or failure based on the overcoming or nonovercoming of ϵ_1 in it. Therefore, in this case, all the time windows are counted as trials.

For each earthquake in the temporal window of completeness, the ShakeMap specifically implemented for Naples is computed; *Faenza et al.* [2013] explain the tools used in terms of ground motion prediction equations and site conditions; these choices are in agreement with the one implemented in the Monte Carlo simulations. These ShakeMaps are calculated including the data available for the event under analysis, the macroseismic field and/or the instrumental records, for the most recent events. We decide to relay on shake maps rather than on raw data since the interpolation scheme used in the ShakeMap code is able to balance and weight different sources of information (e.g., macroseismic and instrumental data, site effects) and to reproduce a shaking field in the dense grid under study. The ShakeMaps are computed in the same dense grid used for the prior model and are evaluated in terms of macroseismic intensity and PGA values, in rock site or using the site amplifications. In practice, we divide the temporally complete part of the catalog into nonoverlapping time windows with a duration ΔT (e.g., 5, 10, and 50 years). For the generic PGA value ϵ_i, we evaluate the number of successes (n_i) and of trials (N_i).

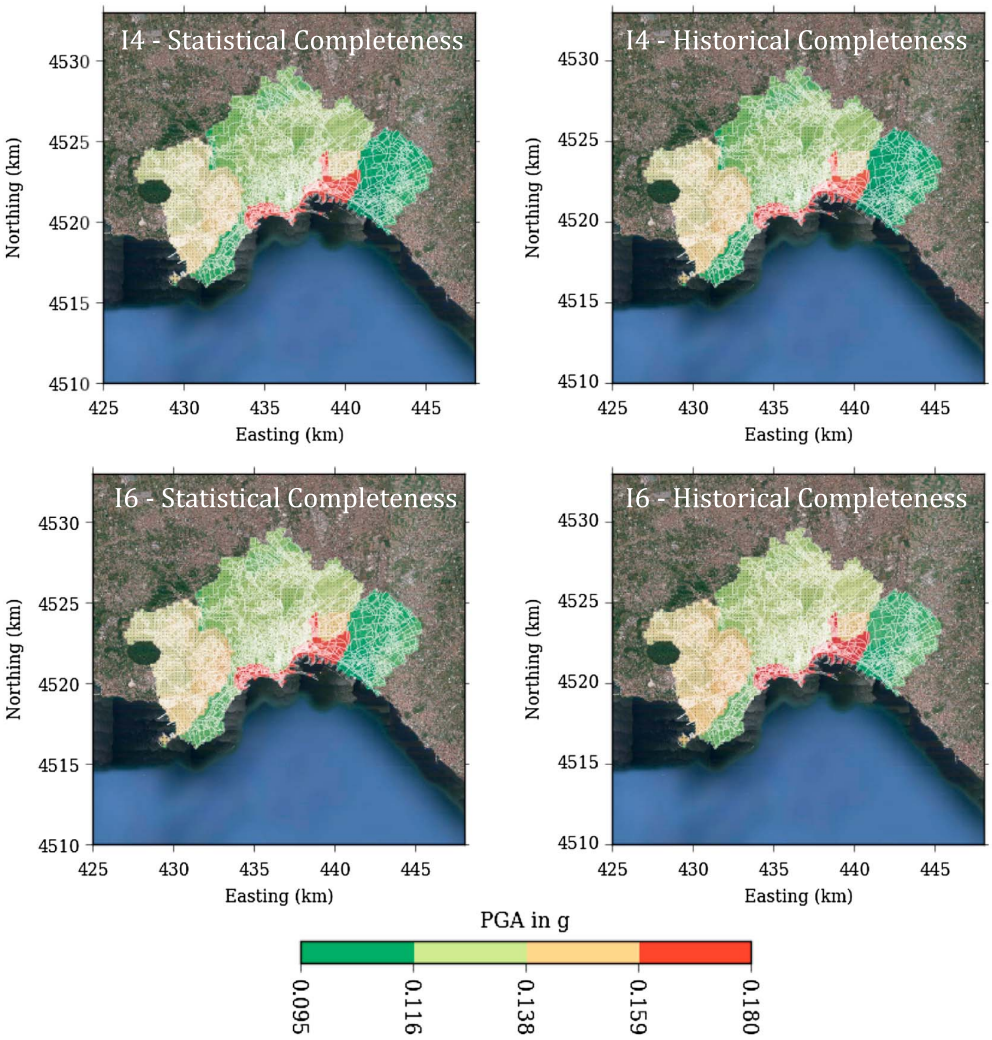

Figure 8. Hazard map as the 10% probability of exceedance in the next 50 years, on the basis of the posterior model using four different likelihood data, including the soil condition.

3.3. The Posterior Distribution and Ensemble Model

To visualize the hazard maps in this Bayesian framework, we adopt a software tool specifically developed to manage, visualize, and compare hazards and risks. The software implementation is similar to what is done in probabilistic volcanic hazard assessment [*Tonini et al.*, 2015]. We evaluate separately the hazard on rock site and with the inclusion of the site condition effect, following the same procedure as in ShakeMap. The results are four posterior distributions, then merged together using an ensemble model, where each model has the same weight. The adoption of the ensemble models provides a full description of all outcomes, providing a description of the uncertainties, both the aleatoric and epistemic factors [*Marzocchi et al.*, 2015]. In this framework, the hazard curve of each of the four posterior models (i) represents the exceedance probability of the model Θ_i^ϵ, for the ϵth PGA threshold, with its weight w_i. So $\{\Theta_i^\epsilon, w_i\}$ in the ensemble modeling strategies is a sample of the unknown parent distribution $f(\Theta^\epsilon)$. The definition of $f(\Theta^\epsilon)$ makes use of the Beta distribution, where $\Theta^\epsilon \sim \text{beta}(\alpha, \beta)$, and α and β are related to the average and variance of the Θ^ϵ, derived by the four posterior models. In total, we have derived six different posterior ensemble hazard models, considering the three different exposure times of interest and two different soil conditions. Each of these ensemble models is based on four different likelihood data and five prior models. Figure 6 summarizes the different models used to build up the hazard based on Bayesian inference.

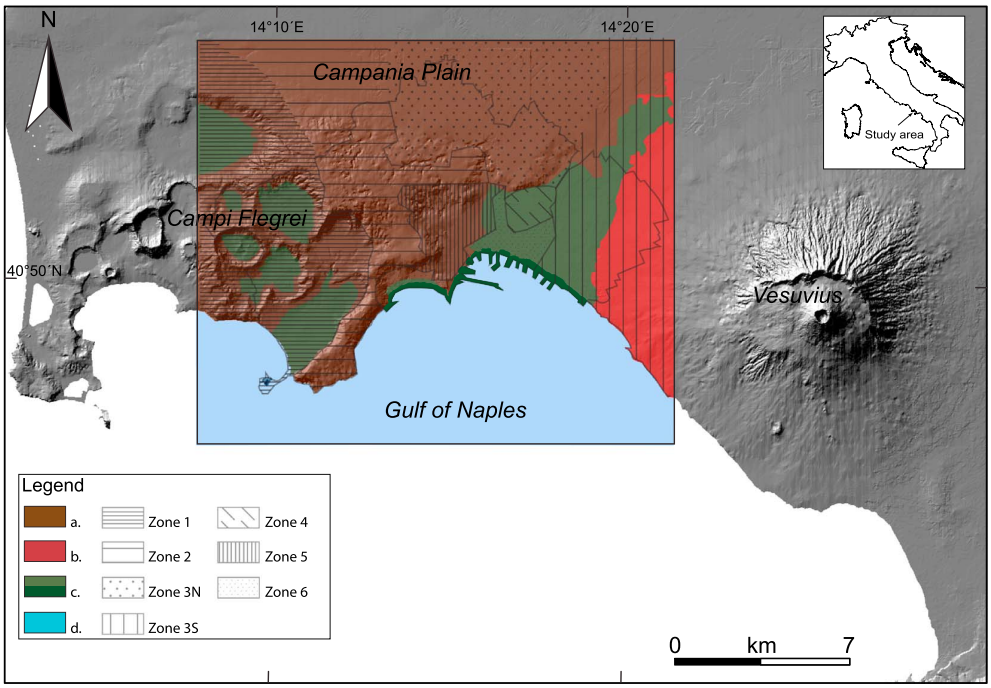

Figure 9. Geological sketch of the study area (bold line). The outcropping deposits have been grouped in three main clusters: (a) Pyroclastic deposits of Campi Flegrei (Ignimbrite Campana deposits and Neapolitan Yellow Tuff); (b) Deposits of Vesuvius; (c) Soil and alluvial pyroclastic deposits (in bright green color) and sea sand (in dark green color); and (d) sea. For our ground-shaking analyses also the deposits of Tyrrhenian Sea have been taken into account. The different patterns indicate the six zones that have been identified and characterized by homogeneous geological deposits on the basis of deep stratigraphic investigation. From *Faenza et al.* [2013].

Once the likelihood has been set up, the posterior distribution is calculated following the conjugacy propriety of the beta distribution [*Gelman et al.*, 2000]. In detail, for each *i*th value of ground shaking ϵ_i, the distribution is

$$\begin{aligned}[\vec{\Theta}_i']^{\text{post}} &= [p(O_i|O_{i-1}]^{\text{post}} \\ &= \text{Beta}(\alpha_i + n_i, \beta_i + N_i - n_i) \\ &= \text{Beta}(\alpha_i + n_i, \beta_i + n_{i-1} - n_i)\end{aligned} \tag{10}$$

It is noteworthy that the inference process allows reduction of the epistemic uncertainty content of prior models by constraining the posterior hazard to the information from past observations. When such data are not available, the epistemic uncertainty of prior models remains untouched. Note also that the decrease in uncertainty gained by including the information from past observations will be larger for low PGA values and smaller for high ones.

Figures 7 and 8 show the hazard maps of 10% of probability of exceedance in 50 years for the four posterior models, based on the four different likelihood data, for rock soil and considering the soil classification. Figure 7 shows an increase in the hazard maps after the inclusion of the past shaking data, for all the four likelihoods. In Figure 8, as already noted in *Faenza et al.* [2013], the role of site effect is dominant. For comparison, Figure 9 shows the site effect adopted in *Faenza et al.* [2013]: it is visible how the hazard maps with amplification effects follow the same patterns as the microzonation. The inclusion of the site effects increases the values of the hazard estimated on rock site, because of the soil amplification factors. This is especially evident in the area of the harbor (zone 4 in the Figure 9), characterized by alluvial pyrochastic deposits and sea sand.

Figure 10 shows the ensemble model of the four posterior distributions for the rock and soil condition, in which the four models are merged into an ensemble [*Marzocchi et al.*, 2015] through a weighted statistical mixing [e.g., *Ray and Lindsay*, 2005] of the four available posterior distributions. In this case, since we do not want to express a preference among the four alternatives, so we set equal weight to all of them. The supporting

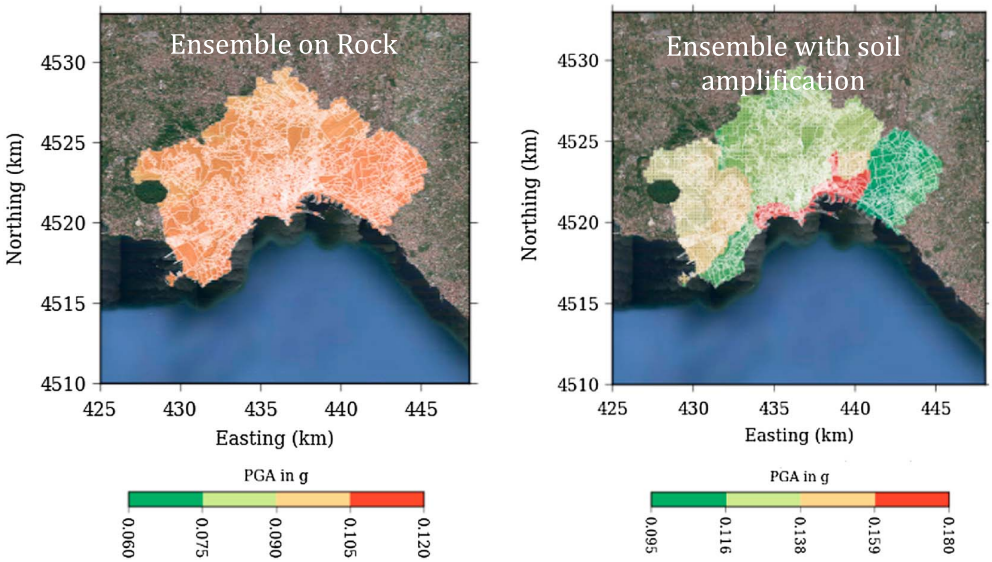

Figure 10. Ensemble model as the 10% probability of exceedance in the next 50 years, for (left) rock type of soil and (right) including soft soil.

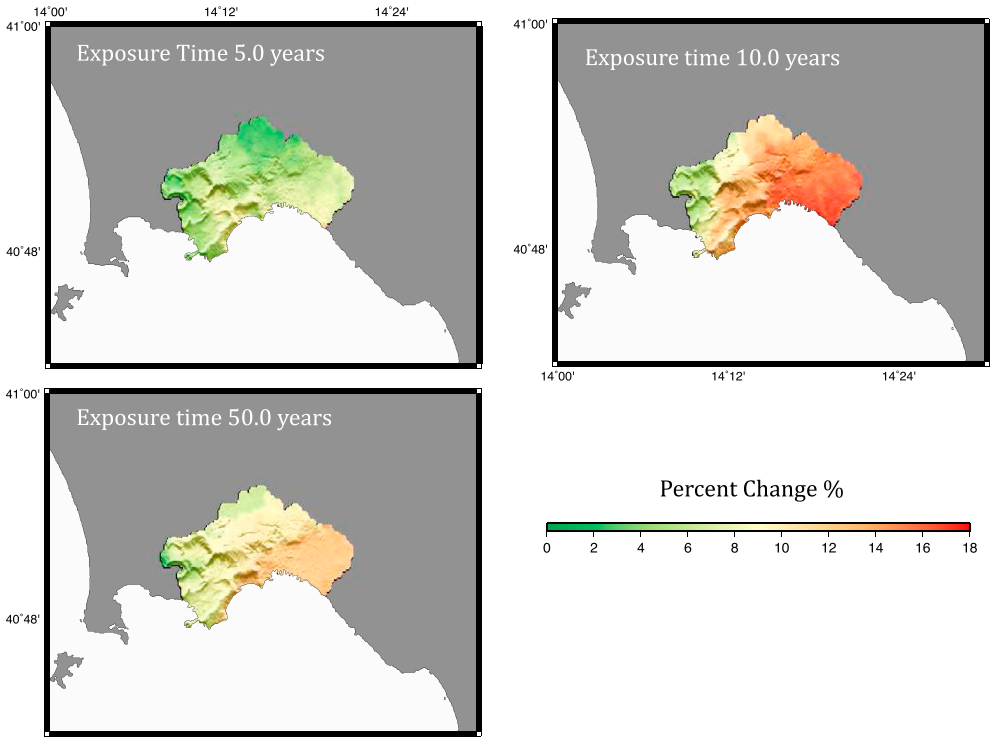

Figure 11. Change of the posterior ensemble hazard maps relative to the prior hazard maps for the three exposure times.

information shows the same analysis but for 5 and 10 years exposure time. The only remarkable difference in the 5 and 10 year analyses, compared to the 50 year one is that the posterior hazards for the intensity I_s6 (both completeness) are smaller compared to the one of intensity I_s4. The reason could be that I_s4 intensity includes smaller events, but closer to Naples, which have not reached the values of I_s6 and with smaller shaking values able to influence the 10% probability of exceedance in 5 and 10 years. Figure 11 compares the hazard of the posterior ensemble model with the one of the prior model (e.g., $\frac{\text{Posterio Ensemble Model}-\text{Prior Model}}{\text{Prior Model}} \times 100$) for the rocky soil. The results show that the inclusion of the past shaking increases the hazard of about 8–10% for the three exposure times.

4. Conclusion

In this work we have applied a Bayesian strategy to calculate the seismic hazard for the city of Naples. We started from the evaluation of the prior models adopting five different statistical models for the earthquake occurrence. We then used the most up-to-date macroseismic data base as likelihood to constrain the prior model, adopting four different temporal-magnitude windows of completeness as likelihood data. Lastly, the four posterior models are combined through the ensemble modeling. The advantage of this approach is the description by means of a pdf of all outcomes of the analysis, with a full description of the aleatory variability and epistemic uncertainties. Remarkably, the hazard values are in line with the ones in MPS04 [*Stucchi et al.*, 2011], even if it is difficult to make a comprehensive comparison of the two products because of the difference in the spatial scale and in the binning of the hazard values. The inclusion of the likelihood data results in an increase of the hazard value of about 8–15% in the hazard maps. The final product of this work can be easily included in the loss estimation analysis adopting the same software tool for the Bayesian analysis.

5. Data and Resources

All data used in this article come from the published sources listed in the references. Some plots are made using Generic Mapping Tools version 4.5.6 [*Wessel and Smith*, 1991; www.soest.hawaii.edu/gmt].

Acknowledgments
The work was supported by the "Futuro in Ricerca 2008" FIRB Project ByMur (RBFR0880SR) financed by MIUR, the Italian Ministry for Research and Education. The authors thank the Associate Editor and the two anonymous referees for the constructive reviews and comments that helped to significantly improve the quality and presentation of our work. Some figures were made using the GMT software [*Wessel and Smith*, 1991; www.soest.hawaii.edu/gmt]. The authors thank all the data sources listed in the references.

References

Akinci, A., F. Galadini, D. Pantosti, M. Petersen, L. Malagnini, and D. Perkins (2009), Effect of time dependence on probabilistic seismic-hazard maps and deaggregation for the Central Apennines, Italy, *Bull. Seismol. Soc. Am.*, *99*(2A), 585–610, doi:10.1785/0120080053.

Akinci, A., D. Perkins, A. M. Lombardi, and R. Basili (2010), Uncertainties in probability of occurrence of strong earthquakes for fault sources in the Central Apennines, Italy, *J. Seismolog.*, *14*, 95–117.

Akkar, S., and J. J. Bommer (2010), Empirical equations for the prediction of PGA, PGV, and spectral accelerations in Europe, the Mediterranean region, and the Middle East, *Seismol. Res. Lett.*, *81*(2), 195–206.

Ang, A., and W. Tang (1975), *Probability Concepts in Engineering Planning and Design, Vol. I: Basic Principles*, John Wiley, U. K.

Armigliato, A., S. Tinti, G. Pagnoni, G. Mastronuzzi, C. Pignatelli, P. Sansó, S. Gallazzi, R. Tonini, and B. Brizuela Reyes (2007), *Studio Preliminare Sulla Sorgente Del Terremoto Del 20 Febbraio 1743 in Puglia Meridionale a Partire Da Dati Di Tsunami*, 26 Convegno Nazionale GNGTS, Roma.

Beauval, C., S. Hainzl, and F. Scherbaum (2006), Probabilistic seismic hazard estimation in low-seismicity regions considering non-Poissonian seismic occurrence, *Geophys. J. Int.*, *164*, 543–550, doi:10.1111/j.1365-246X.2006.02863.x.

Benedetti, L., P. Tapponnier, G. C. P. King, and L. Piccardi (1998), Surface rupture of the 1857 Southern Italian earthquake?, *Terra Nova*, *10*, 206–210.

Cinque, A., A. Ascione, and C. Caiazzo (2000), Distribuzione spaziotemporale e caratterizzazione della fagliazione quaternaria in Appennino meridionale, in *Ricerche del GNDT nel campo della pericolosità sismica (1996–1999)*, edited by F. Galadini, C. Meletti, and A. Rebez, pp. 203–218, Special Publication of CNR-GNDT, Gruppo Nazionale per la Difesa dai Terremoti, Roma.

Console, R., M. Murru, F. Catalli, and G. Falcone (2007), Real time forecasts through an earthquake clustering model constrained by the rate-and-state constitutive law: Comparison with a purely stochastic ETAS model, *Seismol. Res. Lett.*, *78*, 49–56.

Cucci, L., and A. Tertulliani (2010), The Capo Vaticano (Calabria) coastal terraces and the 1905 $M7$ earthquake: The geomorphological signature of regional uplift and coseismic slip in southern Italy, *Terra Nova*, *22*, 378–389.

Del Gaudio, V., P. Pierri, A. Frepoli, G. Calcagnile, N. Venisti, and G. B. Cimini (2007), A critical revision of the seismicity of Northern Apulia (Adriatic microplate–Southern Italy) and implications for the identification of seismogenic structures, *Tectonophysics*, *436*, 9–35.

Deschamps, A., G. Iannaccone, and R. Scarpa (1984), The Umbrian earthquake (Italy) of 19 September 1979, *Ann. Geophys.*, *2*(1), 29–36.

Di Bucci, D., A. Ravaglia, S. Seno, G. Toscani, U. Fracassi, and G. Valensise (2007), Modes of fault reactivation from analogue modeling experiments: Implications for the seismotectonics of the Southern Adriatic foreland (Italy), *Quat. Int.*, *171–172*, 2–13.

Di Bucci, D., B. Massa, M. Tornaghi, and A. Zuppetta (2005), Structural setting of the 1688 Sannio earthquake epicentral area (Southern Italy) from surface and subsurface data, *J. Geodyn.*, *40*, 294–315.

DISS Working Group (2015), Database of Individual Seismogenic Sources (DISS), Version 3.2.0: A compilation of potential sources for earthquakes larger than M 5.5 in Italy and surrounding areas, Istituto Nazionale di Geofisica e Vulcanologia. [Available at http://diss.rm.ingv.it/diss/.]

Faenza, L., S. Hainzl, F. Scherbaum, and C. Beauval (2007), Statistical analysis of time-dependent earthquake occurrence and its impact on hazard in the low seismicity region Lower Rhine Embayment, *Geophys. J. Int.*, *171*(2), 797–806.

Faenza. L., C. Meletti, and L. Sandri (2010), Bayesian inference on earthquake size distribution: A case study in Italy, *Bull. Seismol. Soc. Am.*, *100*(1), 349–363.

Faenza, L., S. Pierdominici, R. Camassi, A. Michelini, E. Ercolani, and V. Lauciani (2013), The shakemap atlas for the city of Naples, Italy, *Seismol. Res. Lett.*, *84*(6), 963–972.
Field, E. H., T. H. Jordan, and C. A. Cornell (2003), OpenSHA. A developing community-modeling environment for seismic hazard analysis, *Seism. Res. Lett.*, *74*, 406–419.
Franza, A. M. (2006), *L'evoluzione Tardo-Quaternaria del Glacis Basale dei Monti di Sarno (Campania) ed il Ruolo Degli Input Piroclastici. Tesi di dottorato*, 286 pp., Università degli Studi di Napoli Federico II, Italy.
Galadini, F., C. Meletti, and E. Vittori (2000), Stato delle conoscenze sulle faglie attive in Italia: Elementi geologici di superficie, in *Le ricerche del GNDT nel campo della pericolosità sismica (1996–1999)*, edited by Galadini et al., pp. 107–136, CNR–Gruppo Nazionale per la Difesa dai Terremoti, Roma.
Galadini, F., C. Meletti, and E. Vittori (2001), Major active faults in Italy: Available surficial data, *Neth. J. Geosci.*, *80*(3–4), 273–296.
Galli, P., and G. Naso (2009), *Unmasking the 1349 Earthquake Source (Southern Italy): Paleoseismological and Archaeoseismological Indications from the Aquae Iuliae Fault*, vol. 31, pp. 128–149.
Galli, P., F. Galadini, and F. Calzoni (2005), Surface faulting in Norcia (central Italy): A paleoseismological perspective, *Tectonophysics*, *403*, 117–130.
Galli, P., V. Bosi, S. Piscitelli, A. Giocoli, and V. Scionti (2006), Late Holocene earthquakes in southern Apennine: Paleoseismology of the Caggiano Fault, *Int. J. Earth Sci. (Geol Rundsch)*, *95*(5), 855–870, doi:10.1007/s00531-005-0066-2.
Gasperini, P., B. Lolli, and G. Vannucci (2013), Empirical calibration of local magnitude data sets versus moment magnitude in Italy, *Bull. Seismol. Soc. Am.*, *103*(4), 2227–2246.
Gelman, A., J. B. Carlin, H. S. Stern, and D. B. Rubin (2000), *Bayesian Data Analysis*, 1st ed., Chapman and Hall/CRC, Boca Raton, Fla.
Giardini, D., S. Wiemer, D. Fäh, and N. Deichmann (2004), *Seismic Hazard Assessment of Switzerland 2004*, Swiss Seismological Service, ETH Zurich.
Grezio, A., W. Marzocchi, L. Sandri, and P. Gasparini (2010), A Bayesian procedure for probabilistic tsunami hazard assessment, *Natural Hazards*, *53*, 159–174, doi:10.1007/s11069-009-9418-8.
Grezio, A., R. Tonini, L. Sandri, S. Pierdominici, and J. Selva (2014), A methodology for a comprehensive probabilistic tsunami hazard assessment: Multiple sources and short-term interactions, *J. Mar. Sci. Eng.*, *3*(1), 23–51, doi:10.3390/jmse3010023.
Grünthal, G., and R. Wahlström (2012), The European-Mediterranean Earthquake Catalogue (EMEC) for the last millennium, *J. Seismolog.*, *16*(3), 535–570.
Gutenberg, B., and C. F. Richter (1944), Frequency of earthquakes in California, *Bull. Seismol. Soc. Am.*, *34*, 185–188.
Kale, O., and S. Akkar (2013), A new procedure for selecting and ranking ground motion prediction equations (GMPEs): The Euclidean distance-based ranking (EDR) method, *Bull. Seismol. Soc. Am.*, *103*(2A), 1069–1084.
ISIDe Working Group (2010), Italian Seismological Instrumental and Parametric Database. [Available at http://iside.rm.ingv.it (last accessed Novembre 2013).]
Locati, M., R. Camassi, and M. Stucchi (2011), DBMI11, the 2011 version of the Italian macroseismic database (in Italian), Milano, Bologna. [Available at http://emidius.mi.ingv.it/DBMI11, last accessed September 2013.]
MacKay, D. J. C. (2003), *Information Theory, Inference, and Learning Algorithms*, 640 pp., Cambridge Univ. Press, New York.
Marzocchi, W., L. Sandri, P. Gasparini, C. G. Newhall, and E. Boschi (2004), Quantifying probabilities of volcanic events: The example of volcanic hazard at Mount Vesuvius, *J. Geophys. Res.*, *109*, B11201, doi:10.1029/2004JB003155.
Marzocchi, W., L. Sandri, and J. Selva (2008), BET_EF: A probabilistic tool for long- and short-term eruption forecasting, *Bull. Volcanol.*, *70*, 623–632, doi:10.1007/s00445-007-0157-y.
Marzocchi, W., M. Taroni, and J. Selva (2015), Accounting for epistemic uncertainty in PSHA: Logic tree and ensemble modeling, *Bull. Seismol. Soc. Am.*, *105*(4), 2151–2159, doi:10.1785/0120140131.
Matthews, M. V., W. L. Ellsworth, and P. A. Reasenberg (2002), A Brownian model for the recurrent earthquakes, *Bull. Seismol. Soc. Am.*, *92*, 2233–2250.
Michetti, A. M., L. Ferreli, E. Esposito, S. Porfido, A. M. Blumetti, E. Vittori, L. Serva, and G. P. Roberts (2000), Ground effects during the 9 September 1998, $M_W = 5.6$, Lauria earthquake and the seismic potential of the "aseismic" Pollino region in Southern Italy, *Seismol. Res. Lett.*, *71*(1), 31–46.
Moro, M., L. Amicucci, F. R. Cinti, F. Doumaz, P. Montone, S. Pierdominici, M. Saroli, S. Stramondo, and B. Di Fiore (2007), Surface evidence of active tectonics along the Pergola-Melandro Fault: A critical issue for the seismogenic potential of the southern Apennines, Italy, *J. Geodyn.*, *44*, 19–32.
Musson, R. M. W. (1999), Probabilistic seismic hazard maps for the North Balkan Region, *Ann. Geofis.*, *42*, 1109–1124.
Ogata, Y. (1988), Statistical models for earthquake occurrence and residual analysis for point processes, *J. Am. Stat. Assoc.*, *83*, 9–27.
Ogata, Y. (1998), Space-time point-process models for earthquake occurrence, *Ann. Inst. Statis. Math.*, *50*, 379–402.
Patacca, E., and P. Scandone (2004), The 1627 Gargano earthquake (Southern Italy): Identification and characterization of the causative fault, *J. Seismol.*, *8*, 259–273.
Pino, N. A., B. Palombo, Ventura G., B. Perniola, and G. Ferrari (2008), Waveform modeling of historical seismograms of the 1930 Irpinia earthquake provides insight on "blind" faulting in Southern Apennines (Italy), *J. Geophys. Res.*, *113*, B05303, doi:10.1029/2007JB005211.
Roselli, P, W Marzocchi, and L Faenza (2016), Toward a new probabilistic framework to score and merge ground-motion prediction equations: The case of the Italian region, *Bull. Seismol. Soc. Am.*, *106*, 720–733, doi:10.1785/0120150057.
Ray, S., and B. G. Lindsay (2005), The topography of multivariate normal mixtures, *Ann. Statist.*, *33*(5), 2042–2065, doi:10.1214/009053605000000417.
Rosenblueth, E. (1964), Probabilistic design to resist earthquakes, *J. Eng. Mech. ASCE*, *90*(EM5), 189–220.
Salvi, S., et al. (1999), A multidisciplinary approach to earthquake research: Implementation of a geochemical geographic information system for the Gargano site, Southern Italy, *Nat. Hazards*, *20*, 255–278.
Scherbaum, F., and N. M. Kuehn (2011), Logic tree branch weights and probabilities: Summing up to one is not enough, *Earthq. Spectra*, *27*(4), 1237–1251.
Scherbaum, F., F. Cotton, and P. Smit (2004), On the use of response spectral reference data for the selection and ranking of ground-motion models for seismic-hazard analysis in regions of moderate seismicity: The case of rock motion, *Bull. Seismol. Soc. Am.*, *94*(6), 2164–2185.
Scherbaum, F., J. J. Bommer, H. Bungum, F. Cotton, and N. A. Abrahamson (2005), Composite ground-motion models and logic trees: Methodology, sensitivities and uncertainties, *Bull. Seismol. Soc. Am.*, *95*(5), 1575–1593.
Scherbaum, F., E. Delavaud, and C. Riggelsen (2009), Model selection in seismic hazard analysis: An information-theoretic perspective, *Bull. Seismol. Soc. Am.*, *99*(6), 3234–3247.
Sirovich, L., and F. Pettenati (2007), *Sorgenti e meccanismi focali di due terremoti distruttivi del 1783 in Calabria dall'inversione dei piani quotati macrosismici*, edited by D. Sleiko, 26° Convegno GNGTS, Rome, Extended Abstract, pp. 105–106, 13–15 Nov.

Selva, J., A. Costa, L. Sandri, G. Macedonio, and W. Marzocchi (2014), Probabilistic short-term volcanic hazard in phases of unrest: A case study for tephra fallout, *J. Geophys. Res. Solid Earth*, *119*, 8805–8826, doi:10.1002/2014JB011252.

Selva, J., and L. Sandri (2013), Probabilistic seismic hazard assessment: Combining Cornell-like approaches and data at sites through Bayesian inferenc, *Bull. Seismol. Soc. Am.*, *103*(3), 1709–1722.

Senior Seismic Hazard Analysis Committee (SSHAC) (1997), Recommendations for probabilistic seismic hazard analysis-guidance on uncertainty and use of experts, U.S. Nuclear Regulatory Commission, NUREG/CR-6372.

Sieberg, A. (1930), Geologie der erdbeben, *Handbuch der Geophysik*, *2*, 552–555.

Smith, W. D. (2003), Earthquake hazard and risk assessment in New Zealand by Monte Carlo methods, *Seism. Res. Lett.*, *74*, 298–304.

Stucchi, M., C. Meletti, V. Montaldo, H. Crowley, G. M. Calvi, and E. Boschi (2011), Seismic hazard assessment (2003–2009) for the Italian building code, *Bull. Seismol. Soc. Am.*, *101*, 1885–1911.

Tonini, R., L. Sandri, and M. A. Thompson (2015), PyBetVH: A Python tool for probabilistic volcanic hazard assessment and for generation of Bayesian hazard curves and maps, *Comput. Geosci.*, *79*, 38–46.

Utsu, T., Y. Ogata, and R. S. Matsuüra (1995), The centenary of the Omori formula for the decay law of aftershock activity, *J. Phys. Earth*, *43*, 1–33.

Vitale, C. (2006), *L'evoluzione morfotettonica plio-quaternaria del sistema Golfo di Salerno-Piana del Sele-Monti Picentini (Appennino Meridionale)*, PhD thesis, Università Degli Studi di Napoli Federico II, Naples, Italy, Università degli Studi di Napoli Federico II. [Open Archive http://www.fedoa.unina.it/639/1/Tesi_Dott._Carmine_Vitale.pdf.]

Wessel, P., and W. H. F. Smith (1991), Free software helps map and display data, *Eos Trans. AGU*, *72*, 441–446.

Woo, G. (1999), *The Mathematics of Natural Catastrophes*, Imperial College Press, London.

Zöller, G. (2013), Convergence of the frequency-magnitude distribution of global earthquakes: Maybe in 200 years, *Geophys. Res. Lett.*, *40*(15), 3873–3877, doi:10.1002/grl.50779.

Zöller, G., M. Holschneider, and S. Hainzl (2013), The maximum earthquake magnitude in a time horizon: Theory and case studies, *Bull. Seismol. Soc. Am.*, *103*(2A), 860–875.

Zhuang, J., Y. Ogata, and D. Vere-Jones (2004), Analyzing earthquake clustering features by using stochastic reconstruction, *J. Geophys. Res.*, *109*, B05301, doi:10.1029/2003JB002879.

Zhuang, J., M. J. Werner, S. Hainzl, D. Harte, and S. Zhou (2011), Basic models of seismicity: Spatiotemporal models, Theme V. Zürich: Community Online Resource for Statistical Seismicity Analysis. [Available at http://www.corssa.org.]

Zhuang, J., D. Harte, M. J. Werner, S. Hainzl, and S. Zhou (2013), Basic models of seismicity: Temporal models. Community Online Resource for Statistical Seismicity Analysis. [Available at http://www.corssa.org.]